Faculty of Technology and Science
Department of Physics and Electrical Engineering

Johanna Rosenlind

The Impulse-Radiating Antenna

Engineering Physics
Master Thesis

Date/Term: 2009-06-12
Supervisor: Prof. Lars Johansson
Mats Jansson
Examiner: Prof. Kjell Magnusson
Serial Number: X-XX XX XX

Karlstads universitet 651 88 Karlstad
Tfn 054-700 10 00 Fax 054-700 14 60
Information@kau.se www.kau.se

The Impulse Radiating Antenna

Abstract

As the interest in intentional electromagnetic interference (IEMI) increases, so does the need of a suitable antenna which endures those demanding conditions. The ultrawideband (UWB) technology provides an elegant way of generating high-voltage UWB pulses which can be used for IEMI. One UWB antenna, invented solely for the purpose of radiating pulses, is the impulse radiating antenna (IRA). In the course of this master thesis work, a suitable geometry of the IRA is suggested, and modelled, for the high-voltage application of 90 kV.

> *... the antennas driven by such pulsers are passive and easy to fabricate since they tend to be a collection of simple conductors, resistors and dielectrics, but can be very complex to analyze via the solution of Maxwell's equations under appropriate boundary conditions.*
>
> C. E. Baum et al., [3]

Contents

List of Figures

Chapter 1

Introduction

This Master of Science thesis work has been performed at BAE Systems Bofors at the department of Applied Physics. It corresponds to 20 weeks of full-time work which is equivalent to 30 ECTS credits or an entire semesters work load. BAE Systems Bofors provide for one supervisor, system engineer Mats Jansson, and Karlstad University provide for yet another, professor Lars Johansson.

1.1 Background

Around the year of 1960, nuclear weapon designers were testing hydrogen bombs, igniting them above the Pacific Ocean. Down below, at the ocean level, the street lights went out at the island of Hawaii. The effect lasted for hours. One might believe it was the direct impact of the bomb that caused the effect. However, it was the induced electromagnetic pulse (EMP) produced by the hydrogen bomb that made it happen.

The phenomena of the street lights provided foundation for a new type of weapons that uses EMP. The weapons affect a target through intentional electromagnetic interference (IEMI). The EMP couple with the target's electronics and induce different effects, such as disturbance or destruction. Lately, technology has made it possible to generate such pulses not using nuclear explosions. One branch of technology which provides this solution is called ultrawideband (UWB) technology. Their line of action is yet more elegant than the generation of an EMP with the hydrogen bomb.

1.2 Problem Formulation

The main technological challenge in implementing UWB technology, is to find an antenna which satisfies the demanding conditions [10]. The UWB antenna is known

for the ultrawideband of frequencies in signal transmission. One identify mainly two ways of developing the antenna. The first is to modify an existing antenna, called the TEM-horn. The second is to develop an entirely new antenna, called the impulse-radiating antenna (IRA). At BAE Systems the first assignment is completed by developing the TEM-horn. A Master's thesis work [33] was performed in 2006, by Monsef Larbi who determined and simulated the specific geometry of the antenna.

My master thesis work will be the natural continuation of the previous work; to perform the research and modelling of the IRA designed for the specific task of UWB transmission, or specifically: An IRA designed for IEMI.

There is already an abundance of well-functioning IRAs. However, the feature which distinguishes the IRA developed during this project is the use of a high-voltage source, *id est* the antenna will be excited with a high-voltage pulse of 90 kV. As a comparison, one other IRA has been developed for high-voltage applications. It operated at the voltage level of 30 kV. [14] 90 kV is three times that of 30 kV, therefore, more sophisticated, high-voltage solutions for the structural components for our IRA need to be considered.

1.3 Objective

In this Master Thesis I will suggest and motivate a suitable geometry for the IRA operating at 90 kV. This is relatively high voltage level which imposes several constraints on the structure. The IRA will be used for IEMI. The antenna will radiate pulses. The pulses are signals with a duration of a few nanoseconds which makes the frequency bandwidth of the signal be of ultrawide character.

1.4 Method

The work was divided into five blocks; research, determination of a modelling software, modelling, construction, and system integration - some of them intersecting.

Initially, a research was conducted. The process had two goals. The main goal of the research was to identify the different parameters that is used as input to the simulation. The subgoal of this block was to grasp the big picture of antenna design and to familiarize the antenna topic.

The second block intersects the first; to find a suitable simulation tool for the relatively complex, electromagnetic configuration. The IRA does not involve traditional configurations. For instance, one cannot make the continuous wave approximation which prevents one from using phasors in the solution of Maxwell's equations. Other features which complicates the choice of simulation tool are the short duration of the pulse and the non-steady-state situation.

Knowing the input parameters and the simulation software, the modelling proceeded. The input parameters was assigned values enabling a hands-on building of the antenna. During this process, entirely new considerations required attention which was either solved or suggested as future work.

In order to initiate the construction of the antenna, the mechanical drawings was developed in close cooperation between myself, my supervisor Mats Jansson and the mechanical designer Erik Loinder. Several overlooked factors emerged to discussion. Nevertheless, the valuable experience of both Mats Jansson and Erik Loinder enables us to find solutions.

Due to unexpected circumstances, the two, final blocks were never initiated. The construction of the IRA and the system integration were postponed to another project in the fall of 2009. Then, the IRA will be built, tested and evaluated. Unfortunately, the results will not be discussed in this master thesis.

1.5 Scope

Within the scope of the master's thesis work I will determine a suitable IRA geometry based on research and modelling, conducting a full-time work load during 20 weeks.

This work will not evaluate the device producing the pulse which is fed into the antenna. I will simply assume that there exists one source which produces a pulse and make an educated guess of the pulse appearance. On the other hand, the properties of the solid state pulse generator, the frequency pulsed generator (FPG 90) will be discussed.

If one knew the appearance of the pulse fed to the antenna, it could be described with a mathematical function. It is then possible to treat the electric far field analytically. Such a treatment would yield an upper bound of the magnitude of the electric field strength. It is then possible to compare the experimental results to those determined analytically. Unfortunately, it is not possible to determine the pulse appearance. The transmitted pulse measured in the far field region does not reveal enough information about the exciting pulse; the antenna alters the appearance to a great extent. To determine the pulse appearance one would need to perform measurements on the FPG 90 which is difficult when the generator solely operates at the 90 kV level.

This work will not evaluate the choice of material in which the antenna is built. In an intellectual experiment one tend to consider the pulse fed to the antenna as high in energy content, making the material choice crucial. A more detailed calculation reveal the contrary. Considering the antenna as a 100 Ω load, the energy fed into the antenna is less than 300 mJ. As a comparison, consider the temperature rise of water, one need 4.18 J to heat 1 g of water one degree Celsius. If the pulse

repetition frequency is higher, the situation is different, but the antenna is fed by a single pulse [30].

The choice of resistors are crucial. During operation there will be high currents passing the resistors. These currents causes an instantaneous heating which causes the resistors, at high enough temperatures, to breakdown. The choice of resistors is a critical process which require an investigation of its own. This is not considered here. In this antenna, we use resistors which have been recommended by experienced and qualified users.

The IRA will operate at a high voltage level. Such an application require certain geometries of the structural components to prohibit the occurrence of electrical breakdown. Suggestions of such geometries are made in this master thesis. But, the quantitative treatment of such an interface is also required; a static voltage excitation of the conductors which suffer from the risk of electrical breakdown, need to be built. The appropriate software for the model is the CST Microwave Studio. The modelling of the areas of the IRA which suffers the risk of electrical breakdown is not performed during this master thesis work.

1.6 Thesis Outline

In chapter 2 the basics of electromagnetism is discussed. Maxwell's equations, the Poynting vector, the Jafimenko's equations and the principle of superposition are the selected topics. Then, the UWB technology is treated from the perspective of main areas of application, the section finishes with the discussion of the UWB antenna. In the following section the IRA is presented; the comprising components, the radiation characteristics, and the diffraction is discussed.

In chapter 3 the optimization of the antenna is discussed by treating the different parts of the IRA individually. The feed arms, the resistive terminations, the feed cable, and the reflector are the different components which require attention. They will be altered to suit IEMI. During antenna operation, there will be an imminent risk of electrical breakdown which clearly apply additional constraints to the geometry. These considerations will thereby be discussed in the chapter. Efficient power transmission is obtained when the different components are matched to each other in the circuit. Thus following the section dealing with the topic of electrical breakdown is a section dealing with impedance matching. The chapter will finish with suggestions of additional components of the IRA which is not included in the IRA developed here, but is still motivated by their serving purpose in the antenna.

Chapter 4 deal with the modelling of the IRA. The chapter will describe the evolution from a primitive model to a smaller, efficient one which provide more accurate results. The results of the modelling will confirm the theoretically, predicted behaviour found during the research of the IRA. Also this chapter will present an

important result regarding the terminating resistance at the junction between the feed arms and the reflector.

Finally, chapter 5 provides a summary and a discussion of the important results. It also describe how to develop my work further.

As for the references, they will be found continuously throughout the text by the use of numbers enclosed in brackets. The bibliography is found in the final chapter.

Chapter 2

Theoretical Framework

The current chapter will provide the theoretical foundation of the electromagnetism in this master thesis. Maxwell's equations states that where there is a changing charge distribution, there will be an electromagnetic field. Jafimenko's equations offer the ability to visualise the electromagnetic fields if one knows the direction of changing current. The ability to determine the appearance of the electric field will help in the modelling of the antenna. knowing the appearance it is possible to add components which enhance or limit certain electric field components. Section 2.1 discuss the basics of electromagnetism. Initially, Maxwell's equations are displayed, then the Poynting vector is applied to the specific example of an coaxial cable, the Jafimenko's equations are listed, along with the principle of superposition which is the property of the electromagnetic field which enables IEMI.

Within the field of UWB technology one uses the theoretical results predicted by the theory of electromagnetism. In Section 2.2 a brief description of the UWB technology is provided focusing on the main areas of application; one being that of IEMI. The section finishes with the characteristics of an UWB antenna.

The IRA will be introduced in Section 2.3. The objective of the section is to describe the IRA in terms of consisting components, radiation properties in both time domain, and frequency domain, and diffractive effects which alter the appearance of the transmitted impulse. The section will introduce the reader to the IRA.

Then section 2.4 will describe the system which enable antenna operation. It is important for the system to operate as one unit which transmit power efficiently. Therefore one regard impedance matching within the system. The components of the system are the solid state pulse generator, the coaxial cable, and the coaxial connector.

2.1 Basic Electromagnetism

The antenna transmits electromagnetic radiation into space. Electromagnetic radiation are electric and magnetic fields caused by charge distributions and currents. The physical processes occurring both inside and outside the antenna during operation are thus governed by the theories of Maxwell and Faraday. The wave model is the main tool for describing the physical processes occurring when the electromagnetic waves are propagating through the transmission lines of the antenna. As for Faraday's concept of electromagnetic fields, it suits the description of the electromagnetic radiation propagating into the antenna's surrounding space. To understand the basics of antenna transmission, along with the effect of electromagnetic interference, an overview of the theory of electromagnetism is found.

2.1.1 Maxwell's Equations

The four equations presenting electromagnetic field theory in a brief manner are called Maxwell's equations; they are derivations made by Heaviside from the early work of Maxwell. They comprise Gauss' law for electricity, Gauss' law for magnetism, Faraday's law of induction and Ampere's circuital law. Explicitly, they read [16]

$$\nabla \times \vec{E} = -\frac{\partial \vec{B}}{\partial t}, \tag{2.1}$$

$$\nabla \times \vec{H} = \vec{J} + \frac{\partial \vec{D}}{\partial t}, \tag{2.2}$$

$$\nabla \cdot \vec{D} = \rho, \tag{2.3}$$

$$\nabla \cdot \vec{B} = 0. \tag{2.4}$$

Where $\vec{E}$ [V/m] and $\vec{H}$ [A/m] are the electric and magnetic field intensity vector, $\vec{D}$ [C/m^2] and $\vec{B}$ [T] are the electric and magnetic flux density vectors, ρ [C/m^3] is the volume density of free charges and $\vec{J}$ [A/m^2] is the density of free currents.

2.1.2 The Poynting Vector

Electromagnetic waves carry electromagnetic power. The rate of such a power transfer is determined by the electric or magnetic field intensities associated with the travelling electromagnetic wave. In a derivation from equations 2.2 and 2.3, one arrive at a vector representing the power flow per unit area; the vector is defined as the Poynting vector $\vec{P}$ and has the explicit expression [16]

$$\vec{P} = \vec{E} \times \vec{H} \ \left[\mathrm{W/m^2}\right]. \tag{2.5}$$

Consider the example the coaxial cable with a transverse electromagnetic wave, propagating through the transmission lines it is possible to determine the power flow per unit area. Let the field intensity vectors be

$$\vec{E} = Ee_r \ [\mathrm{V/m}]\,,$$

$$\vec{H} = He_\theta \ [\mathrm{A/m}]\,.$$

The vectors e_r and e_θ are the radial and angular, unit vectors of the cylindrical coordinates. Then, the Poynting vector is

$$\vec{P} = \begin{vmatrix} e_r & e_\theta & e_z \\ E & 0 & 0 \\ 0 & H & 0 \end{vmatrix} = EHe_z \ \left[\mathrm{W/m^2}\right].$$

Thus, the power flow per unit area inside the coaxial cable defined above will be in the direction along the cable, since the "direction along the cable" are in the e_z-direction.

2.1.3 Jafimenko's Equations

Maxwell's equations are complicated to apply to a complex electromagnetic problem since they require simultaneous solutions of both the time-varying electric and magnetic fields. This favours the use of relations which are functionals of the charge and current density. They are solutions to the Maxwell's equations under the assumption that there exists no other field than those produced by the charge and current distributions. The functionals of the time-varying charge and current distributions are Jafimenko's equations, and read [29] [39]

$$\vec{E} = \frac{1}{4\pi\epsilon_0}\int\left(\frac{[\rho]}{x^2}e_x + \frac{1}{xc}\left[\frac{\partial\rho}{\partial t}\right]e_x - \frac{1}{xc^2}\left[\frac{\partial\vec{J}}{\partial t}\right]\right)dV \ [\mathrm{V/m}]\,, \tag{2.6}$$

$$\vec{H} = \frac{1}{4\pi}\int\left(\frac{\left[\vec{J}\right]\times e_x}{x^2} + \frac{1}{xc}\left[\frac{\partial\vec{J}}{\partial t}\right]\times e_x\right)dV \ [\mathrm{A/m}]\,, \tag{2.7}$$

where both $\rho = \rho\,(t)$ and $\vec{J} = \vec{J}\,(t)$ is time-dependent. The quantities enclosed in brackets are evaluated at retarded time.

Finding explicit expressions for the volume density of charges ρ [C/m^3] and the current distribution $\vec{J}$ [A/m^2] is a difficult task. One normally incorporates a software to enable such a description. However, the benefit from applying Maxwell's and Jafimenko's equations is that one develops a qualitative understanding of the problem. Then, a simulation software provides the quantitative description.

2.1.4 Principle of Superposition

The electric and magnetic fields obey the principle of superposition. This implies that if several fields in space occupy the same region, the net field will have an amplitude equal to the sum of the individual fields. This property applied to electromagnetic waves and fields are called interference.

One distinguish between destructive and constructive interference. The former is the case when the amplitude of the net field will be lower than any of the separate components.

The other type of interference is constructive interference. The amplitude of the net field have a larger amplitude than any of the separate components. As in the case of IEMI. The impact of radiation in a target is that of constructive interference. The radiated electromagnetic field from the antenna will interfere with that of the target and thus induce effects such as voltage surges or currents causing junction breakdown. The target is an electric component of some kind.

The objective of the radiating antenna is either that of constructive interference mentioned above, or by exposing the electrical component to high electric fields, causing breakdown. Such an antenna needs to fulfil certain properties which will be described in greater detail in section 2.2.2.

2.2 The UWB Technology

The objective of this master's thesis work is to implement the UWB technology by the use of short pulses. In such a system the antenna is seen as the most critical component since it operates as a high bandpass filter for the frequencies in the signal, and the system performance is highly dependent upon the antenna performance. The understanding of UWB concepts is essential to grasp the full picture of the application. Thus, an introduction to the topic of UWB will be a natural continuation.

2.2.1 Main Areas of Application

In 2002 the electronic communications committee (ECC) was established with the objective to harmonise the usage of the radio spectrum. They develop a common ground for electronic communication and hence prevent technologies such as UWB to interfere with other technologies. This section will discuss the conditions imposed by the ECC, since they are the regulating authority that govern the commercial UWB usage and control the development of the technique. Then, a few different applications of UWB is discussed, mainly focusing on IEMI.

The ECC has decided not to designate the UWB applications any specific frequency band, which otherwise is the usual way of dealing with devices using the

radio spectrum. Instead they inserted a special clause for the technique; consisting of conditions of usage. For instance, one condition in the usage of devices using UWB technology in the frequency band lower than 10.6 GHz is "that, to reduce interference on outdoor radio stations, it is important to minimise the out door activity of UWB" [17].

Not only do they specify the working conditions for the UWB devices, they also specify the technical requirements for the devices. This means that they assign an upper boundary on the amount of spectral density of the transmitted signal. The spectral density is proportional to the power carried by the signal per unit frequency. The upper boundaries are set as a function of the particular frequency interval.

The conditions imposed on the UWB technology relegates it to indoor, wireless, short-range communication for high data rates, or low data rates for long distances. This makes it suitable for applications such as radar/sensoring and data communication. As for the UWB application developed during this project it does not fulfil the conditions imposed by ECC. The spectral density of the device developed during this master's thesis work does not fulfil the regulations. However the usage of the UWB device occur in a controlled environment. The testing environment is shielded from the environment to prevent interference. Also experiences personal at BAE Systems Bofors will supervise the testing. Therefore, the usage is approved.

Radar and Sensoring

The application of UWB to radar and sensoring has seen progress due to the high time domain resolution. The possibility of pulses in the range of nanoseconds enable a spatial resolution in the extent of centimeters. However, the application is limited by the low spectral power density. This constrains the application to short range radar, such as ground penetrating radar or through walls, indoors.

Data Communication

The success of applying UWB to data communication is understood from the Shannon-Hartley Theorem expressing the channel capacity;

$$C = B\log\left(1 + \frac{S}{N}\right), \tag{2.8}$$

where C is the channel capacity, B the bandwidth, S/N signal-to-noise ratio. The channel capacity is directly proportional to the bandwidth. An increased bandwidth will directly increase the channel capacity. The effect is larger than that of a variation of the other parameters.

The application of UWB to data communication will greatly enhance the performance of both home and office networks, such as WLANs[1] since it enable data rates in the order of Gbps.

Intentional Electromagnetic Interference

The devices used for IEMI are military devices. Therefore, they are allowed to operate on a much greater spectral density level than those used in the civilian market. The regulations imposed on the UWB technology are to prevent devices from interfering. Ironically, that is the purpose of the UWB antenna developed in this project.

The effect due to IEMI on a target is classified into four categories: [27]

- Noise - An applied electromagnetic signal will make the user experience noise in the receiver.
- False information - A designed electromagnetic signal can be designed to feed false information to the receiver.
- Transient upset - It is possible to upset the logic state of the system. The effect is dependent on the system's need to recover after disturbances.
- Permanent damage - For instance, high electric fields will expose the semiconductor junctions to over-voltages with the direct consequence of breakdown.

Transient upset and permanent damage require a higher electric field than does the effects of noise and false information. As for the specific field strengths, they depend on the situation.

2.2.2 UWB Antenna

The feature that distinguishes the UWB antenna from other radiators is the frequency bandwidth; thereby the name, ultrawideband antenna. There are several existing working definitions of the concept of frequency bandwidth. In ref. [39] they offer a definition which is broad but yet not too specific to lose meaning. The definition of the antenna bandwidth is the range of frequencies over which the antenna meets desired specifications. In Figure 2.1 the bandwidth is defined as all frequencies over which the antenna radiation is above 3 dB.

The large bandwidth of the UWB antenna enables it to process signals in a broad frequency range. Prior to the 1950s the broadband antennas had bandwidths not larger than 2:1, which means that the upper frequency of the antenna spectra

[1] Wireless Local Area Network

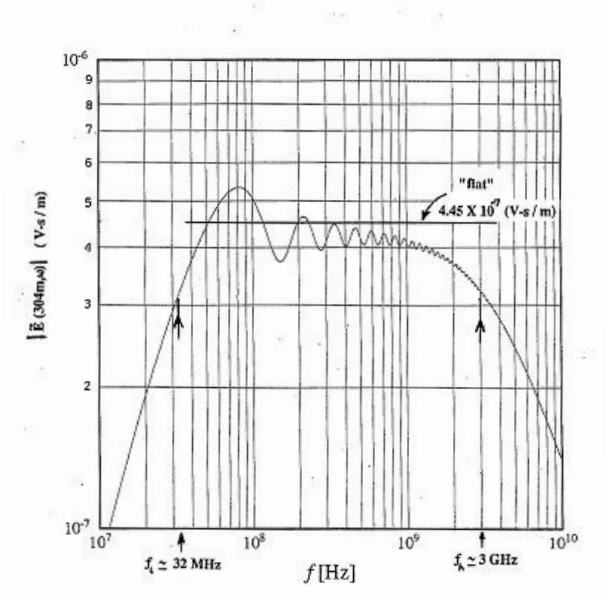

Figure 2.1: The spectral magnitude of a prototype UWB antenna, the IRA displayed in [23]. The bandwidth has been defined as the range of frequencies over which the radiation is above 3 dB which is the point where the magnitude of the electric field is down by a factor of $1/\sqrt{2}$.

is two times that of the lower frequency. However, a breakthrough within the same decade enabled bandwidths in the order of 40:1. Such antennas are usually referenced to as frequency independent since they can operate at such a broad band [2]. The UWB antenna developed during this master's thesis work incorporate some features to improve the frequency independence, such as impedance matching and minimization of diffraction.

In order for a general antenna to qualify as a UWB antenna it should be able to transmit a signal which has a greater frequency bandwidth than 500 MHz;

$$|f_u - f_l| > 500 \text{ MHz}, \tag{2.9}$$

where f_u and f_l denote the upper and the lower frequency of the frequency bandwidth. This definition of the UWB concept is not unique. There are several possible definitions of the UWB concept. One other definition specify the fractional bandwidth of the UWB device. The signal should have a larger fractional bandwidth than 25 %;

$$2\frac{f_h - f_l}{f_h + f_l} > 25\ \%. \tag{2.10}$$

Within the field of our application the former definition (Equation 2.9) has covered more ground and will be the definition used in this thesis.

Due to the large bandwidth of the UWB antenna it is important to make the dispersion of the transmitted signal as small as possible. Dispersion is the stretching and the distortion of the transmitted signal. For the dispersiveless antenna, the relation

$$\lambda f = c \tag{2.11}$$

is fulfilled, where λ [m] is the wavelength, f [Hz] the frequency and c [m/s] is the speed of light; doubling the frequency will cut the wavelength in half [30]. The UWB antenna in this project are known as dispersiveless due to the nature of the transmission lines in combination with the excitation of a TEM wave. This does not imply that the pulse fed to the IRA and the transmitted signal are identical. When the impulse-like signal passes the antenna it will be spread in the time domain. This occurs due to effects such as diffraction, asymmetry in geometry, mismatched resistive loads and impedance mismatch [35]. All which will be discussed further on.

2.3 The Impulse-Radiating Antenna

The impulse radiating antenna (IRA) is the UWB antenna which will be developed during this master thesis work. The most dominating, structural components of the IRA are the reflector and the feed arms which can be seen in Figure 2.2. It also defines two parameters included in the most common metric to characterise a reflector antenna, namely the FD-ratio;

$$\mathrm{FD-ratio} = \frac{F}{D}, \tag{2.12}$$

where F is the focal length and D is the diameter of the reflector. Common values of the quotient belongs to the interval of $0.35 - 0.60$.

Continuing this section, the different components of the IRA will be presented. The components are the reflector, the feed arms and the resistors. They will be discussed both individually and as a single unit during antenna operation. Then, the radiation is treated in the frequency domain to display the ultrawideband characteristic of the IRA, and in the time domain to describe the appearance of the produced impulse. Finally, this section will finish with a discussion of the diffractive effects which alter the appearance of the impulse when the signal passes the antenna.

2.3.1 IRA Components

The IRA has three main components which one need to understand in order to grasp the full picture of IRA transmission. They are seen in Figure 2.2; the reflector, the feed arms (colored grey), and the resistors at the junction between the feed arms and the reflector (light grey). To offer understanding of antenna transmission the components will be treated both individually and as a single unit.

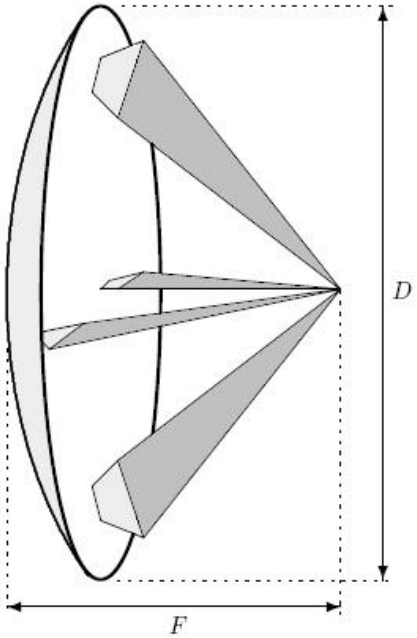

Figure 2.2: Schematic of the IRA. The feed arms and the reflector are the most dominant parts of the geometry. But there are also resistors at the junction between the feed arms and the reflector which highly influence antenna performance.

Reflector

The parabolic reflector is a surface which is known for the characteristic of redirecting an incoming, spherically symmetric wave front into a plane one. The reflector used in this project can be seen in Figure 2.3(a). It has a diameter of 1.8 m and a F/D ratio equal to 0.38. The surface of the reflector is a steel mesh, reducing the reflector weight, compared to the weight of a solid reflector.

The frequencies of the electromagnetic waves is the electromagnetic spectrum. For the specific reflector used in this project, the radiation characteristics on one part of the electromagnetic spectrum has been displayed by issuing the beamwidth of the main lobe of that certain part. A radiation pattern displays graphically the angular dependence of radiation by tracing a curve belonging to one intensity level. In Figure 2.4 one can see a radiation pattern from a directive antenna, such as the IRA. The arrow indicate the direction of the main axis of the antenna, which is also called boresight. At the centre there is a dominating lobe; the main lobe. There are also sidelobes. For the specific reflector used in this project, the width of the main lobe of the C band[2] is 2.915°.

[2]The C band is all frequencies in the interval 0.5 - 1.0 GHz, using the NATO convention.

(a) The reflector used in the construction of the IRA.

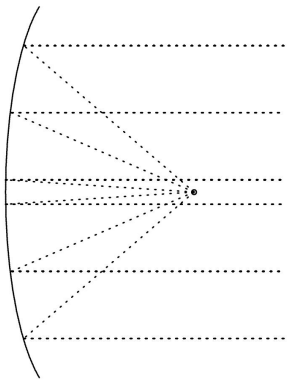

(b) The parabolic surface redirects a spherically symmetric wave into a plane wave.

Figure 2.3: The reflector.

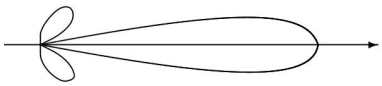

Figure 2.4: A radiation pattern is the angular dependence of the electromagnetic field intensity. The radiation pattern from a highly directive antenna is recognised on the dominating, elongated main lobe. The direction of the the main axis is the boresight of the antenna; outside the main lobe there are side lobes.

Feed Arms

The feed arms are the structural components which make a crossed-like formation on the IRA. They extend from the rim of the reflector to the focal point, supported by some structure at the centre of the reflector. A schematic displaying the feed arm pairs is seen in Figure 2.5. They are made from a metal sheet of aluminium.

At the focal point the feed arms are connected in pairs. As seen in Figure 2.6. Two feed arms of different potential are transmission lines with a varying width and height, called tapered, conical plate transmission lines [26]. They have a characteristic impedance which can be tuned by varying the included feed arm angle; the wider the arm, the lower the impedance. One need to be careful not to make them too wide. A wide feed arm pair cause extensive aperture blockage, limiting the performance of the antenna. As a guideline one can motivate 25 % decrease in impedance of a given set of slim feed arms not to cause too much aperture blockage

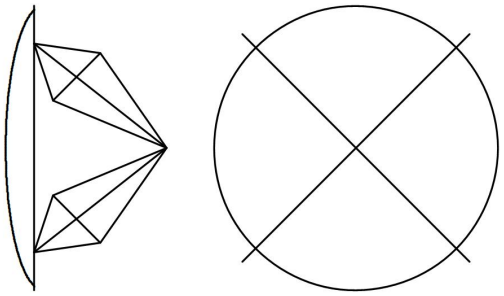

Figure 2.5: The IRA in side- and in frontview.

[18]. The particular characteristic impedance of the feed arm pairs will be discussed further in the next chapter.

It is a known fact [39] that the surface currents during operation will concentrate along the edges of the feed arms. Therefore, it is important to keep the feed arm edge as clean as possible from defects and supporting structures not to disturb the varying charge distributions. Otherwise the diffraction would be severe. Also it is important to avoid sharp edges close to the feed point. Charges tend to build up in those areas which increases the risk of electrical breakdown. This will be described in Section 3.5.

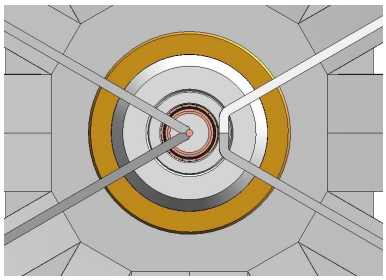

Figure 2.6: The feed arms meets at the focal point and are connected in pairs.

Resistors

The resistors are positioned at the junctions between the feed arms and the reflector as seen in Figure 2.7. There will be several resistor types and configurations tested. The choice of resistor type was based on experience; in projects involving pulses the TFS series has proven reliable. The TFS series are manufactured by Ohmite. Other resistors with the same manufacturer, also recommended, is the TL series and the Maxi Mox.

As for the configuration of the resistors, there will be two alternatives tested; either the single load or the distributed load. The formerly-mentioned comprise a single high voltage resistor placed at the junction between the feed arm and the reflector. This has proven to be successful [13] especially in the case of the $\pm 30°$,

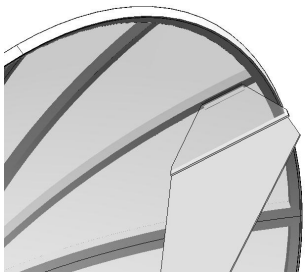

Figure 2.7: The resistors at the junctions between the feed arms and the reflector.

feed arm angle to the vertical which will be discussed further on. The distributed configuration of the resistors has been successfully tested in ref. [13].

The surface currents on the feed arms will concentrate along the edges. It is an important consideration when using the distributive resistor configuration, since it will influence the current carried by each resistor. There has been two distributions up for discussion; not necessarily different from each other. The first distribution of resistors regard high and low resistances. There is always a risk of resistor breakdown due to the relatively high surface currents. In addition the currents tend to concentrate along the edges. Therefore a distributive configuration of resistors with a higher resistance on the strings close to the edges could be a suitable configuration [1]. This configuration has been tested in the past; unfortunately, with the outcome of breakdown of the outermost resistor connection. The application was different from that of the IRA. It motivates the testing of such a configuration.

The second configuration of distributive resistors regards high and low inductances. For the same reason as to distribute higher resistances at the edges, one should distribute the resistors with the higher inductance at the edges as well. In ref. [13] they even add explicit induction to the junction by introducing winded coils. As for the application of the IRA developed during this project, it is to operate at a higher voltage level which add to the risk of electrical breakdown. And a high inductance imply a greater voltage drop across the device [30]. Therefore one cannot be certain that the use of inductive resistors is motivated. But if one consider to try, this is the configuration to use.

To summarize, the particular type of resistors has been recommended by qualified users. The three resistor types are manufactured by Ohmite. They are:

- The TFS series,
- The TL series, and
- The Maxi Mox resistors.

Additional information on each resistor can be found at the manufacturers website.

IRA Operation

This section will describe the above-mentioned components; the feed arms, the reflector, and the resistors during antenna transmission. The excitation will be assumed to emerge from the focal point which is not (at the moment) assumed to be connected to anything. Further, the propagation of the TEM wave to the focal point will be treated in Section 2.4. For now, the TEM wave emerges from nowhere.

During excitation, a voltage difference is applied to each of the feed arm pairs. Induced surface currents on feed arms will propagate along the edges from the focal point towards the reflector rim. Between arms of different potential, this causes a spherically symmetric TEM wave to propagate toward the reflector. The spherically symmetric, electric field is viewed in Figure 2.8.

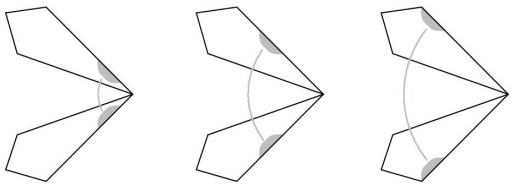

Figure 2.8: The surface currents give rise to the electromagnetic field. Between feed arms of different potential, a spherically symmetric TEM wave will emerge and propagate toward the reflector.

At the reflector rim, the resistors will dissipate the energy which not yet has been radiated. The dissipation minimizes reflections of the TEM wave such that as much energy as possible is radiated. The remaining charge distribution on the feed arm pairs will simply vanish when distributed on the reflector surface.

This straightforward process of antenna transmission will be optimized in the course of this master's thesis work. Design principles which will be considered are the impedance matching of the different components; the avoidance of electrical breakdown due to the high-voltage application; and minimization of diffractive effects.

2.3.2 Radiation Characteristics

The IRA is known for generating an impulse in the far field region. The impulse is ultra wide in frequency domain and extremely narrow in time domain. From the two perspectives of frequency domain and time domain, the radiation from the IRA will be described.

Frequency Domain Radiation

To establish the UWB properties of the IRA it is possible to analyse the IRA in frequency domain and study the spectral magnitude of the electric field. A plot reveals the UWB properties. In ref. [23] it was shown that it is possible for the bandwidth of the IRA to be within the range from 32 MHz to 3 GHz, certainly qualifying for UWB. A similar analysis has been made for the IRA developed during this project.

The input voltage waveform is assumed to be equal to that of the voltage waveform launched by the generator, which reads [30]

$$V(t) = V_0 \left(e^{-\beta t} - e^{-\alpha t}\right) \ [\mathrm{V}], \tag{2.13}$$

as is visualised in Figure 2.9, where V_0 is a scalar, α^{-1} [s] is the time of rise and β^{-1} $[s]$ is the time of decay of the voltage pulse.

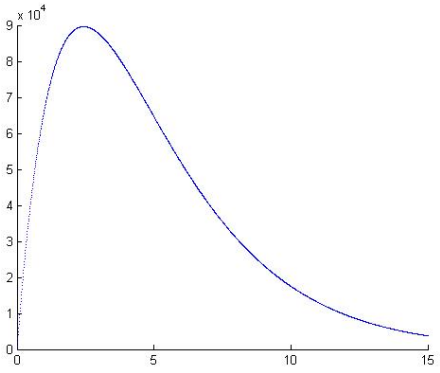

Figure 2.9: A plot of Equation 2.13. The voltage [V] as a function of time [ns] of the voltage waveform launched on the antenna by the FPG 90 generator. The scalar V_0 is adjusted such that the peak voltage is 90 kV.

Then, the spectral magnitude of the radiated electric field is [23]

$$E_M(\omega) = \frac{\sqrt{2}D}{4\pi c f_g}\frac{V_0}{r}\left[1 - \frac{2\sin(\omega T)}{\omega T} + \frac{\sin^2(\omega T/2)}{(\omega T/2)^2}\right]^{1/2} \frac{\omega(\alpha-\beta)}{\sqrt{\beta^2+\omega^2}\sqrt{\alpha^2+\omega^2}} \ [\mathrm{V/m}], \tag{2.14}$$

where D [m] is the reflector diameter, c [m/s] is the speed of light, f_g the geometrical impedance factor, r [m] the distance from the antenna, α^{-1} $[s]$ is the rise time, β^{-1} $[s]$ is the time of decay, and

$$T = \frac{2F}{c} \ [s]. \tag{2.15}$$

Numerically, for our IRA, the numerical values of the parameters are listed in Table 2.1.

The spectral magnitude of the IRA can be seen in Figure 2.10(a); in Figure 2.10(b) we have the spectral magnitude of the prototype IRA evaluated in the article [23]. The spectral magnitudes differ due to several reasons.

Table 2.1: The numerical values of the parameters in Equation 2.14 for the IRA developed here.

Parameter	Numerical value
D	1.8 m,
$V_0{}^3$	
c	3 10^8 m/s,
α^{-1}	2 ns,
β^{-1}	3 ns,
r	5 m,
f_g	0.54, and
F	668 mm.

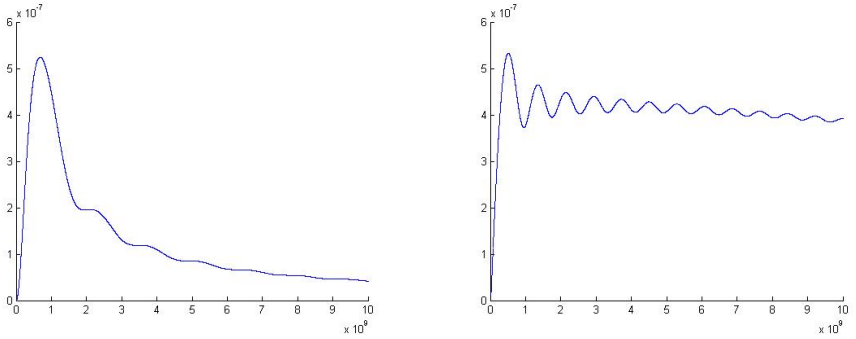

(a) The IRA developed here.

(b) The prototype IRA presented in ref. [23].

Figure 2.10: The spectral magnitude of the electric field as a function of frequency.

- First, the time of decay is supposed to be a lot longer than that of the time of rise of the voltage waveform. Comparing the IRA and the prototype IRA, $\beta_{IRA} < \beta$, we see that the time of decay of the pulse launched on the IRA is shorter than that of the prototype. However, it is longer than that of the time of rise. We assume it is enough to apply the model.

- Second, comparing the diameters of the prototype IRA and the IRA developed here, $D = 3.6$ m and $D = 1.8$ m, we realise that the prototype is scaled with a factor of 2. It certainly influences the result.

- Third, the input antenna impedance differ, which makes the geometrical impedance factor differ. Later in this master thesis the geometrical impedance

factor will be treated in greater detail. By now it is enough to know that this has an effect of the radiated field.

Even if the spectral magnitude of the radiated field of the IRA is much smaller than that of the prototype IRA found in ref. [23] it still qualifies as a UWB antenna since it has a greater bandwidth than 500 MHz.

Time Domain Radiation

The traditional way of analysing general antenna radiation is to only treat the frequency domain, as has been done in the preceding paragraph. However, a function in frequency domain can be represented in time domain, and vice versa. The transition between the two is as follows. Let $f(t)$ be an integrable function on $\mathbf{R}$. The representation in frequency domain is the Fourier transform $\hat{f}(\omega)$ on $\mathbf{R}$ reads [22]

$$\hat{f}(\omega) = \int e^{-i\omega x} f(x)\, dx. \tag{2.16}$$

The time domain representation of the same function reads [22]

$$f(t) = \frac{1}{2\pi} \int e^{i\omega x} \hat{f}(\omega)\, d\omega. \tag{2.17}$$

Due to the short pulses and UWB character of the antenna the analysis is more easily done in time domain. Despite the manifestation of the IRAs UWB properties, all other analyses will thus be performed in time domain. For instance, time domain characteristics such as the prepulse, impulse and tail of the IRA radiation will be explained further on in this section.

When the antenna is in operation the solid state pulse generator launches an impulse. It propagates through the feed as a spherically symmetric wave onto the reflector. Which, in turn, redirects the beam, such that the IRA radiates a planar wave into the far field region. One generally uses the terms near-field and far-field region when discussing radiation. Generally expressed, they are regions in space in which one can make certain mathematical approximations; having boundaries which are vaguely defined. For this master thesis it is enough to know that the radiation will have certain characteristics in each region.

The pulse radiated from the antenna has a characteristic shape, as seen in Figure 2.11. The different stages of the radiation is called prepulse, impulse and tail. The prepulse having a negative sign originating directly from the feed in the direction of the observer. Followed by the positive impulse; initiating after a time step equal to twice the focal length divided by the speed of light. Finally, the tail of the pulse reach the observer. The tail is not always negative as in Figure 2.11. It can also be

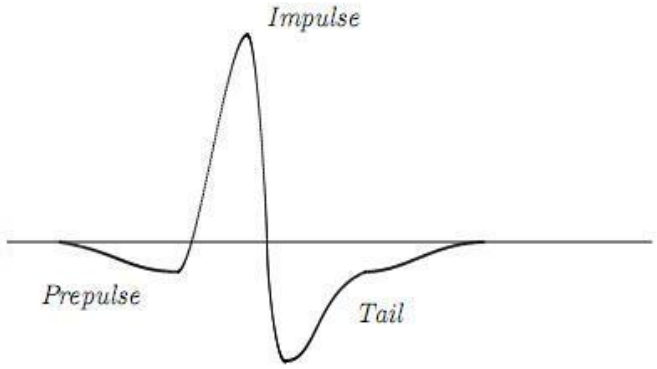

Figure 2.11: A schematic of the on-axis radiation from an IRA. The observer is standing far to the left in the image and will observe the prepulse, impulse and the tail of the radiation, in that specific order.

of oscillating nature, and is highly influenced by the electric and magnetic dipole moments which will be treated further on.

The entire pulse is limited by constraints. The first time-integral of the entire pulse should be zero. And, the second time-integral should be proportional to the late-time dipole moment. The constraints are summarized in [24] as,

$$\int_{-\infty}^{\infty} \vec{E}\,(r,t)\,dt = 0, \tag{2.18}$$

$$\int_{-\infty}^{\infty}\int_{-\infty}^{t} \vec{E}\,(r,t')\,dt'dt = -\frac{\mu_0}{4\pi r}\left[\vec{p}\,(\infty) - \frac{e_x}{c}\times\vec{m}\,(\infty)\right]. \tag{2.19}$$

Due to the constraints one want the tail of radiation to decay rapidly. Otherwise it might oscillate to a great extent and then decrease the radiated impulse. To accomplish the rapid decay of the tail one adjusts the electric and magnetic dipole moments; something that will be described further on in the following chapter.

2.3.3 Diffraction

The IRA is dispersiveless in the sense that the transmission lines of the antenna does not alter the signal during transmission. However, the radiated signal is not identical to the signal fed by the solid state pulse generator. The alteration of the signal arises from diffraction. On the IRA, diffraction occur mainly due to three interactions. The interactions are between the electric field and either

- the edge of the feed arms,
- the feed arms themselves, or
- the reflector rim.

Each interaction will be treated individually.

The spherically symmetric TEM wave which is redirected by the reflector will encounter the feed arm edge as it propagates into the far field region. Initially, the TEM wave encounter the feed arm edge. This induces a surface current which is expressed and integrated in [24] to obtain an expression of the electric field in the far field region. From the expression it is possible to deduce the effect of the interaction. Hence, the feed edge interaction contributes to the initial dip in the postpulse occurring just after the impulse.

As for the interaction between the TEM field with the feed arms, the total current on the feed arms are important; one does not distinguish between the total current on the feed arms and the surface currents on the edges as in the previously mentioned interaction. Thus, the total current on the feed arms has been integrated in ref. [24] to obtain an expression for the electric field in the far field region. One sees that this effect makes a negative contribution to the field at a later time than that of the effect from the edge diffraction.

The two, previously mentioned interactions are similar in the way that they contribute to the diffractive effects. Currents on the feed arms give rise to an electric field in the far field region. The interaction between the electromagnetic field and the reflector rim differ in the sense that the surface currents are induced on the reflector. It is also different in the sense that it makes a positive contribution to the electric far field. The TEM field is parallel to the reflector rim. The effect of this interaction is positive and occur in later time than those mentioned above [24].

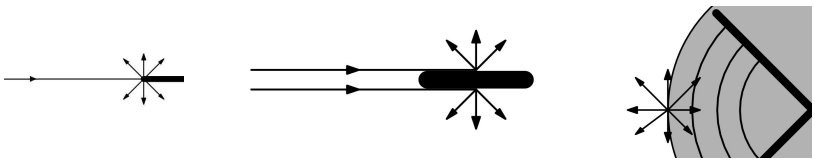

(a) The interaction between the incoming TEM wave and the feed arm edge.

(b) The interaction between the incoming TEM wave and the feed arms.

(c) The interaction between the wavefront and the reflector rim.

Figure 2.12: The arrows visualize the incoming and diffracted radiation.

The diffractive effects are undesired. They alter the appearance of the postpulse by either adding positive or negative components. It is possible to minimize the effect by the use of thin feed arms. Unfortunately, one will always encounter diffraction dealing with real-world systems.

2.4 The System

In Section 2.3, the different components of the IRA was treated both individually and as one single unit. Now, this perspective will be broadened. The IRA will be treated as a single unit in the circuit consisting of the solid state pulse generator, the coaxial cable and the antenna itself. Also in this section, the TEM wave which was earlier assumed to arise from nowhere at the focal point, will get a more rigid treatment.

The Coaxial Cable

In the system there are two coaxial cables. There is the cable running from the solid state pulse generator to the coaxial connector at the rear of the IRA, with the characteristic impedance of 100 Ω. There is another 75 Ω-cable mounted at the center of the reflector running from the connector to the feed point of the IRA. In this section the properties of the coaxial cable will be displayed along with important design considerations, such as cable bendings and the dimensions of the cable.

The coaxial cable in Figure 2.13 consists of two coaxially-mounted, cylindrical conductors; separated by a dielectric. The conductors are made from copper and the dielectric is a polymer filling the void between the conductors.

Figure 2.13: A cross section of the coaxial cable. Both the inner and the outer conductor is visible, along with the dielectric filling the void between the two. A rubber shield sits on the outside to protect the cable and the surrounding.

The impulse will propagate inside the cables onto the antenna. The impulse is a TEM wave, as shown in Figure 2.14. Using cylindrical coordinates, the electric field is in the positive, radial direction. The magnetic field is, assuming that the z-axis is directed out from the paper, in the positive angular direction.

Ideally the propagating TEM wave exists only between the inner and the outer conductor. But in real-world devices there is defects in the structure, causing some of the fields to "spill out" and extend outside the outer conductor; making it necessary to include an outer shield. This shield is usually made of rubber. The shielding plastics protects the surrounding from the cable. It is also the other way around,

the shielding protects the fields inside the cable from the surrounding. The interference from the environment of the transmitted signal is decreased. For the specific application of the IRA, one has found success in adding more shielding protection in the form of ferrite beads on the feed cable. These chokes will limit the occurrence of unwanted surface currents on the outer conductor of the coaxial cable.

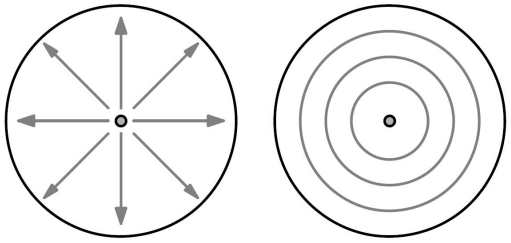

Figure 2.14: The TEM wave inside the coaxial cable. To the left one sees the electrical field component of the wave which is in the radial direction. To the right, the magnetic field component is in the angular direction. Assuming one considers cylindrical coordinates.

When the launched pulse propagates along the coaxial cable one needs a rapid response from the cable not to delay the signal. The unit step response which is the time for the coaxial cable to respond to a rising step in the voltage, is [7]

$$\operatorname{erfc}\left(\left[\frac{\tau}{t}\right]^{\frac{1}{2}}\right)u\left(t\right). \tag{2.20}$$

Where t [s] is time,

$$\tau = \left(\frac{z}{4}\frac{\Xi}{Z_{c0}}\right)^2, \tag{2.21}$$

Z_{c0} is characteristic impedance of the cable, z cable length,

$$\Xi = \frac{1}{2\pi r_i}\left[\frac{\mu_i}{\sigma_i}\right]^{1/2} + \frac{1}{2\pi r_o}\left[\frac{\mu_o}{\sigma_o}\right]^{1/2} \left[\mathrm{H/Sm}\right], \tag{2.22}$$

r_i [m] inner conductor radius, r_o [m] inner radius of outer conductor, μ [H/m] permeability of the media, and σ [S/m] conductivity of the media.

A plot of equation 2.20 in Figure 2.15, for different radii of the coaxial cable, reveal the benefits from a larger, outer conductor radius. Namely, a larger radius enables a more rapid unit response. One should always keep the coaxial cable radius as large as possible not to delay the signal. Unfortunately, the larger cable radius is in conflict with the preferred geometry for aperture blockage, namely, a small cable diameter near the feed point not to disturb symmetry. In this balance we have chosen to emphasize the larger cable radius. The reason for this is not solely the more rapid unit response but is also advantageous for avoiding electrical breakdown, described later in Section 3.5.

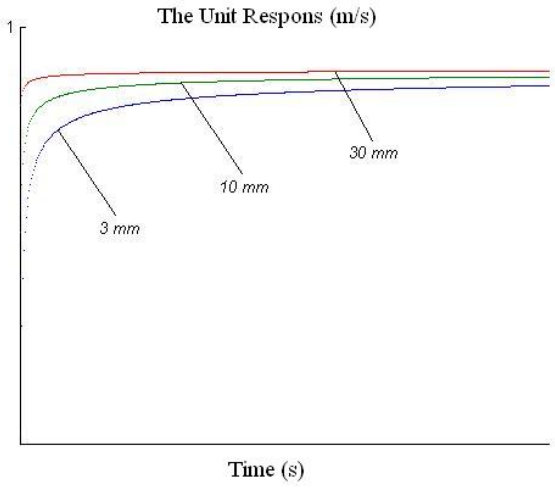

Figure 2.15: The graphical representation of the unit response with respect to time of coaxial cables with different inner diameters of the outer coaxial cable; 3 mm, 10 mm and 30 mm. It is clear that the coaxial cable with the largest outer diameter has the most rapid unit response.

The Coaxial Connector

At the rear of the reflector the coaxial cable connector is mounted. The connector is seen in Figure 2.16. On one side it connects the IRA to the coaxial cable from the generator. At the other side the inner conductor of the coaxial at the center of the IRA is electrically connected by soldering to the metal piece at the center of the connector; the outer conductor is connected to the outer conductor of the cable.

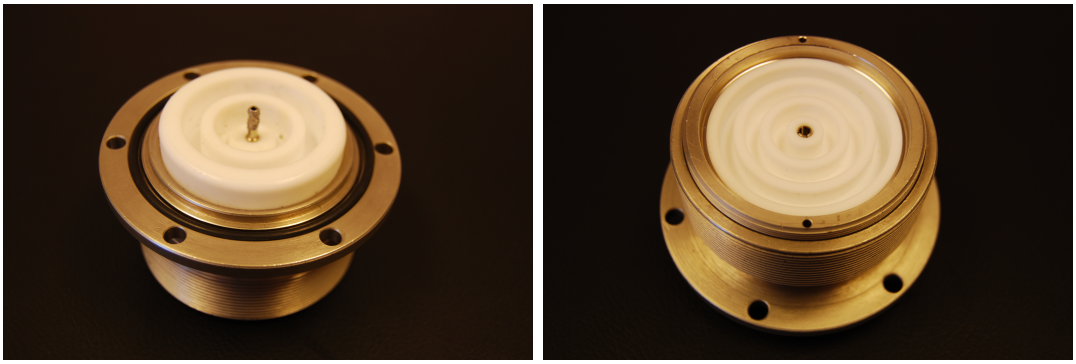

Figure 2.16: The flange-mounted coaxial connector.

It is important to match the impedance of the connector to that of the circuit in order to minimize reflections. The connector has an impedance somewhere in the range 75-100 Ω. It is not possible to be more specific due to the lack of information from the manufacturer.

The connector is built for high-voltage applications. The outer and inner conductor is separated by a larger distance than usual and a dielectric material having a

specific shape, preventing the phenomena of surface electrical breakdown occurring when the IRA is in operation.

As for the connection of the 100 Ω-cable to the coaxial connect, the metal surface on the sides of the connector has a threaded shape to provide a rigid connection. It is sensitive to vibrations and wear which would cause poor connector performance. Most types has specified the number of times they can connect/disconnect the connector and still expect it to operate in a certain way.

The Solid State Pulse Generator

The solid state pulse generator (the FPG 90) excites the IRA. The generator in use is a member of the FPG-N series, manufactured by the German company FID GmbH. It produces a voltage pulse which is a few nanosecond in duration. More specifically, it has a rise time within 1-2 nanoseconds and a pulse width of 1-3 nanoseconds, a maximum pulse repetition frequency of 1 kHz and an operating voltage of 90 kV.

From the FPG 90 there is a coaxial cable connecting to the IRA through a connector at the rear of the antenna. The coaxial cable and the connector has matched impedances of 100 Ω. In the centre of the antenna there is one coaxial cable from the connector to the apex of the IRA. Unfortunately, this cable has an impedance different from 100 Ω namely a characteristic impedance of 75 Ω. At the junction between the connector and the cable there will be an impedance discontinuity. At the discontinuity, reflections will occur during operation. The reflections are undesired, since they directly imply losses in electrical power. In addition they can also destroy the FPG 90, if the reflected wave propagates into the device and if the generator is not properly grounded. However, there are ways to overcome this unwanted effect.

Regard the IRA as a load in a circuit represented by a particular impedance; either larger or smaller than that of the FPG 90. Then, it is possible to match the generator to the IRA by the addition of resistors; either in series or in parallel to the antenna. This will tune the effective impedance of the IRA-resistor subsystem to match that of the FPG 90 and thus lower the reflections. Another technique to deal with the reflections is back matching. Then the generator is configured to operate at a specific impedance level called the output impedance. This is either a property of the generator itself or it can be accompanied by adding resistors in parallel to obtain the correct level. Reflections from a mismatched load are then absorbed by the output impedance of the FPG 90. This is the most common technique and is most probable in use in our generator. The output impedance of the FPG 90 is 100 Ω.

It is difficult to deduce the voltage waveform of the voltage pulse produced by the FPG 90. Earlier we approximated the voltage waveform when performing the spectral magnitude calculation by the use of a double exponential. It is a

good approximation. To be certain of the waveform, this need to be confirmed by measurements. This imposes another difficulty since the FPG 90 produce a non-adjustable static voltage pulse. Due to the high voltage peak of the pulse, any measurements on the generator is difficult since components in the test setup tend to breakdown. In other projects which has been mentioned during discussions [30, 1], has suffered from resistor breakdown due to the instantaneous heating of the device. Therefore, testing of the FPG 90 was not performed.

Chapter 3

Optimizing Performance

The components of the IRA has been introduced in the previous chapter; the resistors, the feed arms and the reflector. In the present chapter the components will be discussed from the viewpoint of optimization. Obviously, the components highly influences antenna performance. They need to work smoothly together in operation as a single unit. This smooth cooperation is obtained if the components are matched with regard to impedance. A methodology on how this impedance matching is performed will be discussed in this chapter.

The Sections 3.5 and 3.6 deals with the important considerations of electronic breakdown and impedance matching. Due to the high voltage excitation it is important to prohibit electrical breakdown in areas of the IRA where the conductors of different potential are close to each other. And in order to establish an efficient power transmission throughout the circuit, the impedance of the components need to match.

The components of the IRA are adjusted to suit the specific application for which the antenna is developed. In the IRA developed during this project, our objective is to maximize the magnitude of the electric field strength on boresight. In our application we have chosen to exclude two most commonly used IRA-components; the ground plane and the splitter. However, they will be discussed in this chapter due to their serving purpose in many IRAs.

As was discussed in Section 2.2 the UWB antenna is highly suitable for the application of radar and sensoring. As for the IRA this is not always true when it has proven not to succeed in the preservation of the transmitted and received signal due to crosspolarization. Therefore a lot of work has been done in the area of preventing crosspolarization of the transmitted and received signal. The ground plane is one component which suppress crosspolarization. Due to it's important role in the IRA it will be treated here.

The inclusion of a ground plane allows for the usage of only half the IRA. This configuration is called half impulse radiating antenna (HIRA). It is a possible

alternative to the IRA developed here. The HIRA has the advantage of speeding the testing process, in terms of mounting of different resistor configurations when one only needs to make two, instead of four. Due to the importance of the HIRA it will be treated as one possible alternative to the IRA developed during this project. One need the ground plane in order to obtain HIRA operation, therefore the presentation of the HIRA is included in the discussion of the ground plane.

As for the splitter balun, the importance of the component is realised when one regard the impedance matching between the coaxial cable and the feed arm transmission lines. Common impedance values of the coaxial cable require a relatively wide set of feed arms. But the wide feed arms are undesired due to the aperture blockage which they give rise to. Using a splitter, one obtain "better" impedance values which match to relatively slim feed arms. To clarify the terminology, for the IRA developed during this project, we will not use a splitter in the traditional sense. There will be one device at the focal point which divide the signal from the coaxial cable into the transmission lines. In Section 3.6 this device is called the splitter. But a more suitable term for the device is a "transition", however it is called a splitter.

The splitter balun and the ground plane are components which enhance antenna performance. The reason for including them into this chapter is merely to make the reader aware of their serving purpose in the antenna. By including the discussion of the components into this chapter the reader realises that these are components which will enhance the antenna performance further.

3.1 Feed Arms

The importance of impedance matching was discussed in the previous chapter. If not carried out, a significant portion of the transferred power is lost due to reflections at the impedance discontinuities. The feed arms are the transmission lines from the feed point to the reflector. They need the appropriate characteristic impedance not to cause power losses in the circuit.

The characteristic impedance of the feed arms are dependent on the included angle of the feed arms. For a given feed impedance it is possible to adjust the included angle of the feed arms such that they become an appropriate impedance match to the feed point. In the optimization process one consider several factors of the feed arms, namely

- the angle which the feed arms make with the vertical ϕ_1 symmetry line of the IRA, in Figure 3.1(a),

- the included angle of the feed arms ϕ_2, in Figure 3.1(b), and

- the radial position of the feed arms on the reflector ϕ_3, in Figure 3.1(c).

All effects will be discussed in this section.

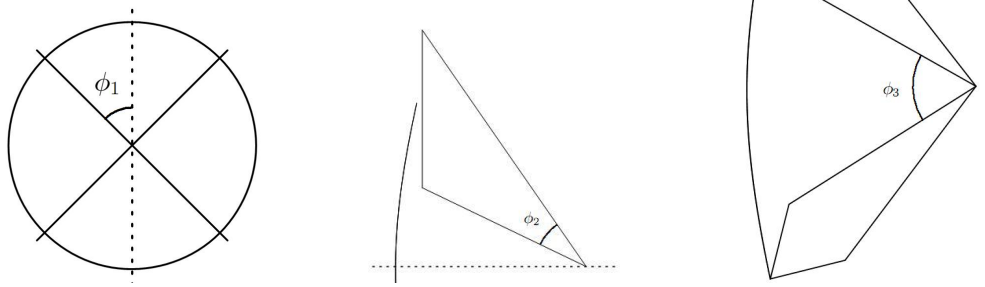

(a) The angle made with the vertical symmetry line.

(b) The included angle of the feed arms. The line which define the feed arms are elongated to emphasize the angle.

(c) The radial position of the feed arms on the reflector.

Figure 3.1: The three angles of optimization.

The angle which the feed arms make with the vertical affect the dipole moments governing the radiation of the IRA. Early designs of the antenna had feed arms positioned $\pm 45°$ to the vertical due to symmetry considerations. In [5] and [41] they suggest the angle $\pm 30°$. It was later confirmed in [13] that this made an improvement to IRA performance. A positioning of this kind enabled a higher effective gain, a higher aperture efficiency and a better crosspolarization rejection[1] . The effect becomes more noticeable when moving to higher frequencies. The proved improvement of antenna performance due to the $\pm 30°$ angle of the feed arms to the vertical motivates the use of such an angle in the IRA developed for this project.

Another effect of the placement of the feed arms, to the $\pm 30°$ angle, were additional reflections shown in the TDR [12]. This effect is not as important in our application since we are interested in improving the gain of the antenna. In other applications, such as radar, the effect of the reflections is more severe. The reflections makes a nonexisting target to appear on the screen.

The feed arms are the transmission lines from the feed point to the reflector. For the specific configuration of four arms with the angle of $\pm 45°$ to the vertical the characteristic impedance of one transmission line is [4, 41]

$$Z_c = f_g Z_0, \tag{3.1}$$

[1]Crosspolarization rejection of an antenna is the ability to preserve different polarizations of the transmitted signal.

where f_g is the geometrical impedance factor, and Z_0 [Ω] is the impedance of free space. The geometrical impedance factor is given by the expression

$$f_g = \frac{K(m)}{2K(1-m)}, \tag{3.2}$$

where K are the complete elliptical integrals with values found in [37], and the parameter m is determined by the geometry of the feed arms, namely

$$m = \frac{b_1^2}{b_2^2}, \tag{3.3}$$

and b_1 and b_2 are defined in Figure 3.2.

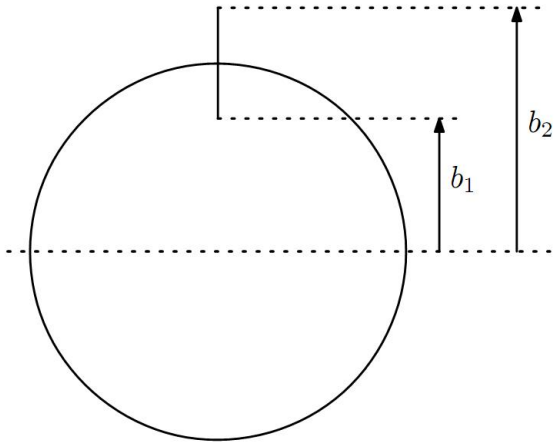

Figure 3.2: The reflector with the two measures defining the included angle of the feed arms; the parameters b_1 and b_2.

The IRA developed for this project will have a 30° angle to the vertical, different from the 45° angle mentioned above. But it is still possible to design the feed arms such that the impedance of the transmission line is matched to the circuit, by the use of the method displayed above. In the article [41] they provide a graphical representation of the plate widths as a function of the angle to obtain the correct value for the feed impedance.

Using the graph in Figure 3.3, for the angle 30° and the feed impedance 150 Ω (the coaxial cable is split into two transmission lines which should have the impedance 150 Ω each) one can identify the value of the quotient, which is

$$\frac{b_1}{a} = 0.82, \tag{3.4}$$

where a [m] is the radius of the reflector. The radius $a = 900$ mm implies that $b_1 = 738$ mm. Then using the fact that the IRA is a self reciprocal antenna we have [19, 41]

$$a = \sqrt{b_1 b_2} \tag{3.5}$$

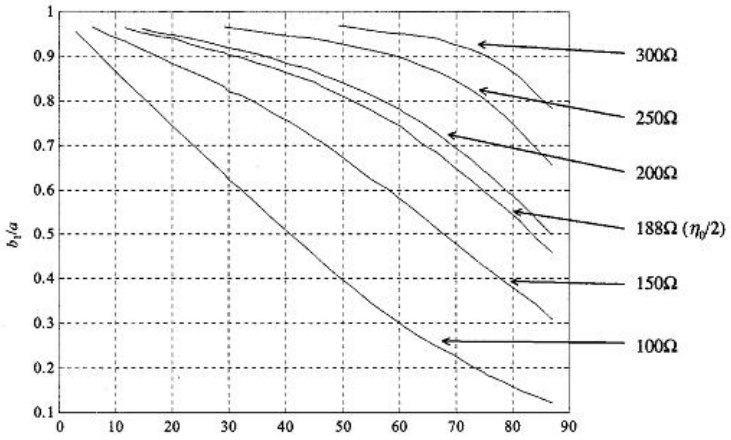

Figure 3.3: The plate widths as a function of the feed arm angle made with the vertical for certain values of feed impedances. The parameter a [m] is the radius of the reflector. [41]

which implies that

$$b_2 = 1098 \text{ mm}. \tag{3.6}$$

To summarize, the included angle of the feed arms are specified by the parameter values $b_1 = 738$ mm and $b_2 = 1098$ mm.

The final alteration of the feed arms are the displacement of the feed arm termination closer to the reflector. By doing this, one focuses the electric field towards the centre of the reflector and thus minimizes some diffraction caused by the rim of the reflector. However, one cannot move the arms too close to the centre. A part of this focused electric field give rise to an unwanted electric field component in the far field region.

In ref. [42] they performed experiments were they moved the feed arms closer to the centre of the reflector. Along with this they also excluded a part of the aperture giving rise to the unwanted electric field components. They found that moving the feed arms affected the aperture height negatively, an overall decrease of 7%. However, a combination of moving the feed arms and excluding the portion of the aperture field that gave rise to the unwanted electric field components had only a negligible effect compared to the original configuration. The combination only lowered the aperture height with 0.4 %. Moving the feed arms closer to the centre is motivated by the use of feed arms constructed by some conducting fabric. Then, the feed arms need to be contained within the radius of a circular reflector.

To summarize, the included feed arm angle is adjusted according to the parameters b_1 and b_2, this will make the transmission lines match the overall circuit. The angle made with the vertical will be 30° due to the proven enhancement of the electric field strength. Also, the feed arms should not be radially displaced.

3.2 Resistive Terminations

At the junction between the feed arms and the reflector there are resistors. The usage of these are three-fold; to minimize reflections visible in the TDR, to drain the charges which are built up in the area, and to align the electric and magnetic dipole moment in order to obtain the optimal radiation properties of the antenna. The first two mentioned are understood but the alignment of the electric and magnetic dipole moment requires more treatment. It will be explained here.

The ideal radiator is discussed above. If the radiator has the electric dipole $\vec{p}$ and the magnetic dipole $\vec{m}$ placed perpendicular to each other, and if their magnitude are related by the relation

$$p = \frac{m}{c},$$

where c are the speed of light, m is the magnitude of the magnetic dipole, and p is the magnitude of the electric dipole, then this radiator is called an ideal p cross m radiator. Its radiation has some specific features: [21]

- The radiation pattern is rotationally symmetric with the direction of maximum radiation as its rotational axis,
- there will only be purely real power out flowing from any spherical surface enclosing the source region, and
- it will have twice the directivity of a purely electric or magnetic dipole.

The radiator described is the ideal case which one desires due to its superior radiation properties. As for the reflector this situation is theoretically possible to obtain; long focal lengths relative the reflector diameter affects the symmetry and gives the vector orientations the proper alignment. However, for realistic antennas the quotient $\frac{F}{D}$ is too small.

The electric dipole moment arise from the accumulation of charge which is instantaneously built up during operation at the junction between the feed arms and the reflector. A higher resistance limits more charges from escaping the feed arms onto the reflector and thus increase the strength of the electric dipole. As for the magnetic dipole, it arise from the current in the feed arm-reflector circuit. A higher resistance of the terminations enables an increased current in the circuit. Hence the strength of the magnetic dipole decreases with a higher resistance.

With knowledge about the dipole moments one can design an optimal matching network to be inserted at the junction between the feed and the reflector. In ref. [25] they provide a methodology on how to determine the electric dipole moment with the input parameter being the characteristic impedance of the feed horn. In theory this is an appropriate approach. But in practice, one tunes the terminating impedance by regarding the TDR of the antenna.

3.3 Feed Cable

The feed cable is the 75 Ω, coaxial cable ranging from the center of the reflector to the focal point. In the IRA developed here, the coaxial cable is placed inside a pipe made by some dielectric. In many IRAs the feed cable is not positioned on the axis at the center of the IRA. For those configurations the coaxial cable passes the rim of the reflector and is placed on one of the feed arms to avoid the capacitive connection between the reflector and the coaxial cable at the center of the reflector [8]. This cause exterior currents in the outer conductor of the coaxial cable which, in turn, give rise to one diffractive electric field component. However, the construction of the antenna feed becomes simpler if one places it on the center axis which motivates our construction.

As for the feed cable mounted on the feed arms; the ideal geometry of the antenna does not have such cables along the feed arm which disrupt the perfect, symmetric structure. Near the rim of the reflector the effect of such cables on the geometry is small. But as one moves along the feed arm into the focal point, the feed arm geometry is greatly reduced and the coaxial cable is in that region the dominant structure. See Figure 3.4. This imposes a perturbation to the otherwise ideal geometry, a perturbation that will scatter the fields and lower the antenna efficiency.

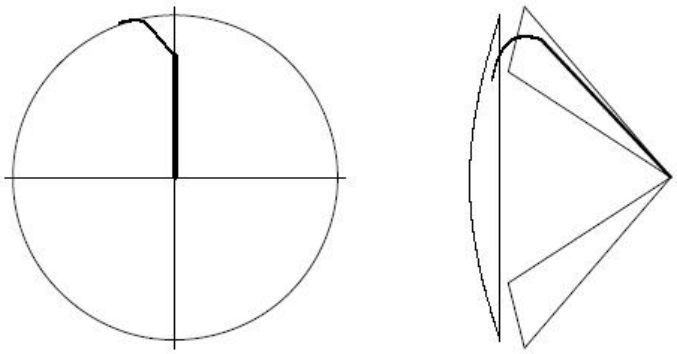

Figure 3.4: A schematic of how the feed cable affects the overall geometry. Closer to the rim, the feed cable is small compared to the feed arm. But as one moved closer to the centre, the feed cable becomes the dominant part of the structure.

Another way of dealing with large cables close to the apex is to use coaxial cables with a varying diameter; a smaller diameter in those regions where the cables are the dominant, structural feature. A smaller diameter will reduce the time response of the cables, which is the reason for not using it all over the antenna.

3.4 Reflector

The reflector used in the construction of the IRA is a steel beam design supporting a mesh seen in Figure 2.3(a). It has a diameter of 1.8 m and a F/D ratio equal to 0.38. When we were measuring the metrics of the reflector, trying to compare it to a paraboloid surface defined with the similar dimensions, we found that the deviation of the reflector from the paraboloid surface was relatively large. This consideration required attention, to reveal the influence of the deviation on the overall radiation performance.

The deviation of the reflector from the paraboloid surface with the measures $D = 1.8$ m and $F/D = 0.38$ causes a displaced focal point. This could be critical, depending on the frequency interval of interest. If the focal point is displaced, either toward or away from the reflector, the radiation from the antenna will diverge. This will decrease both the antenna gain and the directivity[2]. The effect is seen in Figure 3.4. This motivates for a more thorough investigation of how the focal point displacement affect the IRA in our application.

Analytically, the focal length has been determined in ref. [28] for the case of a paraboloid reflector with an infinitesimal electric dipole as feed. The dependence of the electric field on boresight on the displacement of the focal point is seen in Figure 3.6.

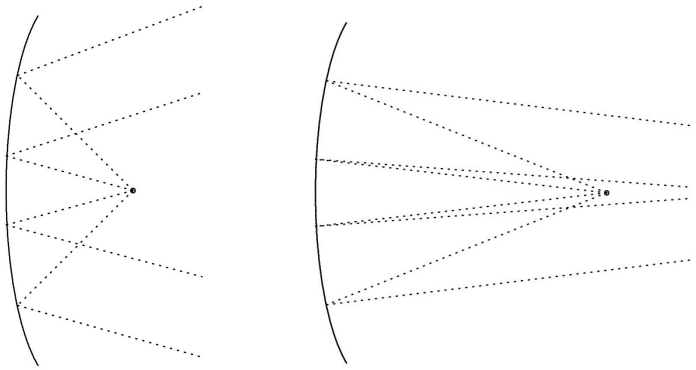

(a) The focal point is displaced toward the reflector.

(b) The focal point is displaced away from the reflector.

Figure 3.5: Focal point displacement.

It can be assumed that the analytically-determined model of ref. [28] can be applied to our specific application. This is a fairly good approximation since the

[2]The definition of directivity is "the ratio of the radiation intensity in a given direction from the antenna to the radiation intensity averaged over all directions." [2]

model offer an upper bound of the electric field strength when the reflector in the article is fed by an electric dipole and will not suffer from aperture blockage caused by the feed arms. The wave length interval of interest is $0.15 - 300$ m which is equivalent to the spectral interval of $1\text{MHz} - 2$ GHz. According to Figure 3.6 found in [28] a displacement of 15 cm would cause the electric field on boresight to decrease with 50 % for the particular frequency of 2 GHz. As for our antenna, the spectral magnitude of the electric field has a peak at 1 GHz (which will be shown further on). At this frequency, a displacement of 30 cm would decrease the field with 50 %. But 30 cm is a large displacement, our concern was that the focal point needed to be determined within a few millimetres, not to lower antenna performance. As one understands, the focal length is to be determined within a few centimeters, not to loose too much of the electric field on boresight. However, the focal length is not the critical parameter of this antenna.

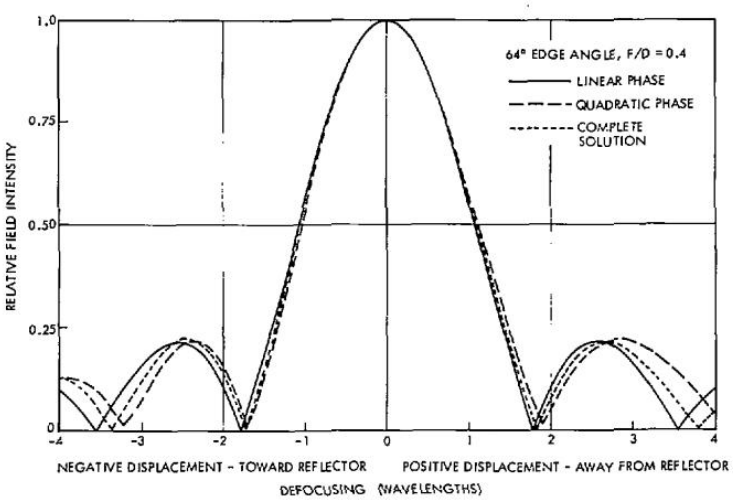

Figure 3.6: A graphical representation of the effect of a displaced focal point. The electric field intensity relative boresight is displayed as a function of a displaced focal point. The unit on the x-axis is wavelengths.

Other features of the IRA developed during this project also conform to the conclusion of an antenna not sensitive to focal point displacement. The highly tapered feed arms and that the spectral operation will be limited to low frequencies, enables the antenna not to be sensitive to a displaced focal point.

3.5 Electrical Breakdown

High-voltage applications impose challenges on the structural components. The risk of electrical breakdown, breakdown due to the relatively high voltage difference between two conductors is imminent in different parts of the IRA. In this Section the difference between several such principles will be discussed. They are surface breakdown, volume breakdown and breakdown in gas.

At the feed point there is a risk of surface electrical breakdown. The combined dielectric interfaces between the polymer of the coaxial cable and the open air is a critical area. The high-voltage difference between the conductors are 90 kV. Between the conductors free electrons might escape the metal and form a conductive path between the two. Along the path, the emerging current will cause a discharge and thus cause electrical breakdown. The critical metric is the distance between the cathode and the anode which should be kept sufficiently large. A correctly designed interface will decrease the probability of such breakdown. The interface maximizes the length between the anode and the cathode.

The conductive path emerges when electrons propagate from the cathode to the anode. It takes that path a finite time to form. One needs a potential difference to remain a sufficiently long time for the path to build up. Since we are dealing with a pulsed course of action, the potential difference will be present only a few nanoseconds. Therefore, the risk of surface breakdown is lower compared to the situation of a constant, permanent, potential difference.

The interface at the feed point needs a design which maximizes the distance between the cathode and the anode. A threaded shape on the interface is preferred where the threads are deep such as those in Figure 3.7. The reason for the deep threads are that electrons will propagate fast across the radial stretch. But along the axis of the cable, the electrons propagates in a slower pace; due to the direction of the electric field, which is in the radial direction. Along the electric field the electrons propagate faster than perpendicular to it.

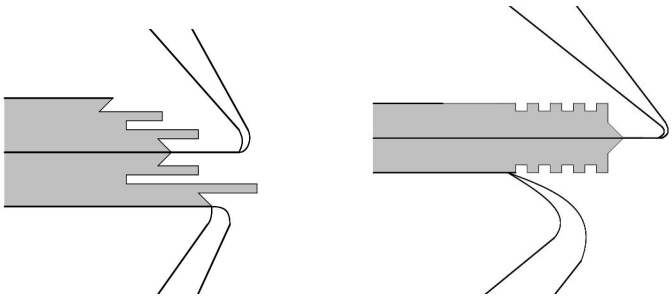

Figure 3.7: Suggestions of the combined interface between the polymer inside the coaxial cable and air. These configurations lengthen the distance on the surface between the anode and the cathode.

Volume electrical breakdown occur inside materials. The part of the IRA suffering the risk of volume breakdown is the dielectric in the coaxial cable. Inside such a material there are defects. They have a lower dielectric strength than the surrounding material if they are arranged in a way that enables for the build-up of a conductive path between the cathode and the anode as seen in Figure 3.8 [32]. If the defects are such that they are elongated in the direction of the electric field, this

causes breakdown. To avoid the occurrence of volume breakdown inside the coaxial cable not only should one use a cable designed for the high-voltage applications, the cable should also have a low defect density.

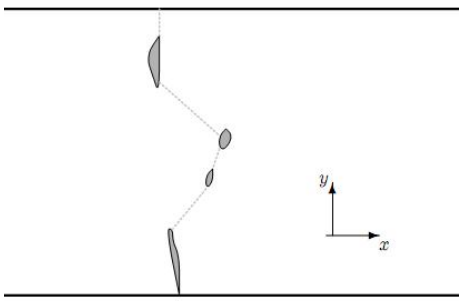

Figure 3.8: A conductive path (dashed) is formed in an area with a high defect density. The electric field is in the y-direction. Therefore, defects which are elongated in the y-direction cause more likely electrical breakdown than do those elongated in the x-direction.

The electrical breakdown of a gas is similar to that of the volume breakdown. The difference is the state of the matter in which the conductive path is built up. The conductive path between the anode and the cathode is seen as a corona at discharge. The dielectric strength of air is normally set to 25 kV/mm. The potential difference between two conductors will be 90 kV. Taking into account the effect of reflections one realises that the highest potential difference will be around 110-120 kV [31]. This makes the critical distance between two conductors equal to

$$\frac{120}{25} = 4.8\text{mm}. \tag{3.7}$$

The antenna is driven with one pulse with a duration of a few nanoseconds. Since the process of electrical breakdown is time dependent, the short pulse is to our advantage. The quantitative extent of this effect is difficult to determine but one can be certain that if we construct an antenna with the shortest distance between two conductors of 4.8 mm the electrical breakdown of air will most certainly not occur. If the distance need to be made smaller than this value it is possible to cover the system with a container and then fill it with a gas with a higher dielectric strength. For instance, the gas SF_6 has a higher dielectric strength than air. It used to be suitable for such usage. Lately, it has been settled that SF_6 has a large impact on the environment and is thus banned from the market.

To be certain of the non-electrical breakdown assumptions one can build an electrostatic model of the interfaces in softwares such as CST Microwave Studio or COMSOL Multiphysics. A static voltage excitation on the conductors will then tell if the electric fields become too large at the critical areas of the construction. Thereafter, one can make certain adjustments to obtain the most suitable configuration. This is not within the scope of this master's thesis work. One attempt was made. However, the computer in my office could not manage the software.

3.6 Impedance Matching

Throughout this chapter the topic of impedance matching is mentioned several times. It is an important topic which highly influences antenna performance. If one designs an antenna with a good impedance matching one can be certain that the power transmission from the source will be as effective as possible. In Figure 3.9 the different transmission lines of the antenna circuit is seen. The designated parameters are the voltage of the source V, the internal impedance of the source Z_i, the 100 Ω, coaxial cable T_1, the 75 Ω, coaxial cable T_2, the splitter S, the two feed arm pairs T_3 and T_4, the terminating impedances T_{31}, T_{32}, T_{41}, and T_{42}.

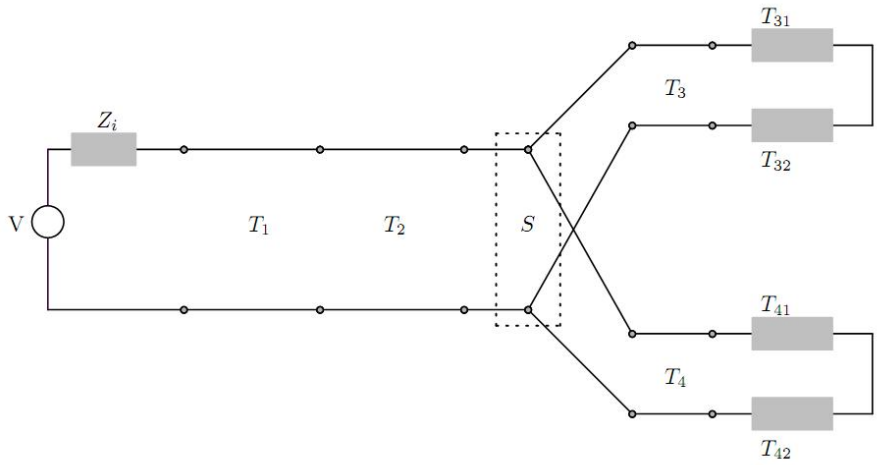

Figure 3.9: The transmission lines of the system.

Consider the TEM wave produced by the FPG 90 generator. The pulse is transmitted from the 100 Ω generator into the 100 Ω, coaxial cable. The transmitted wave will not encounter any obstacles until it meets the impedance mismatch at the second, 75 Ω, coaxial cable. The junction between the two coaxial cables introduces an impedance discontinuity where a portion of the wave will be reflected back, and thus cause power loss. For a TEM wave, power loss is equivalent to a decrease in the voltage associated with the TEM wave. The reflection coefficient of the junction is

$$\Gamma = \frac{75 - 100}{75 + 100} \approx -0.14. \tag{3.8}$$

The voltage amplitude of the reflected wave caused by an incoming wave with amplitude V_i is

$$V_r = \Gamma V_i. \tag{3.9}$$

Unfortunately, one will lose about 14% of the voltage amplitude of the TEM wave at the impedance mismatch.

Moving on, inside the circuit, the TEM wave will propagate from the 75 Ω cable, divide between the feed arm pairs, while passing the area of the focal point of the IRA. The feed arm pairs are approximately considered as tapered, conical plate transmission lines with a characteristic impedance given by equation 3.1 which is discussed in the next chapter. The arms will be adjusted such that the impedance mismatch at the focal point will be as small as possible. The procedure will be described in the next chapter.

Unfortunately, the transition from the 75 Ω, coaxial cable to the feed arm pairs is vaguely defined in terms of impedance. The transition region manifest a splitter from the 75 Ω-cable to the 150 Ω-transmission lines. There will be severe reflections at this point in the circuit. To make the transition smoother the outer conductor could be truncated at an angle which lower reflections. But the risk of electrical breakdown is far more severe than the occurrence of reflections. Therefore the appearance of the transition between the coaxial cable and the feed arm pair will be governed by the prohibition of electrical breakdown.

At the end of the feed arms, the TEM wave will face the terminating impedances T_{31}, T_{32}, T_{41}, and T_{42}. The impedances can be chosen such that they are equal to

$$\frac{T_3}{2} = \frac{T_4}{2}; \tag{3.10}$$

since the terminating resistances are connected in series connected through the reflector. Such a termination will minimize the reflections in the circuit and thus make the radiation tail, discussed in Section 2.3, decay rapidly. Unfortunately, such a terminating impedance align the electric and magnetic dipoles in an unfavourable way. A more sophisticated choice is to prefer [24]. In [25] they determine the electric dipole moment of an IRA. As for the magnetic dipole moment, it will be calculated in the future. When one can determine both the electric and magnetic dipole moment it is possible to determine the terminating impedance numerically. For now, one use the TDR to determine the most favourable impedance. As for the IRA developed during this project, the choice of terminating impedance will be governed by the functioning with the high voltage impulse. The resistors need to be able to withstand the instantaneous heating caused by the produced impulse.

3.7 Additional Components

The IRA developed during this project will incorporate components such as feed arms, resistors and one reflector. Unfortunately, it will exclude interesting devices such as the ground plane and the splitter balun. These devices have shown to

provide improved antenna performance and will therefore require the attention of this section. The discussion of the ground plane also treats the version of the IRA which only incorporates half the reflector and two of the feed arm; the half impulse-radiating antenna (HIRA).

3.7.1 Ground Plane

Consider the IRA seen in Figure 3.10. The ground plane is inserted horizontally on the reflector. The feed arms are connected to the plane. The feed arm pair above the plane has a positive potential relative the lower one. At the reflector rim the field lines follow the circular structure at the arc between the arms. At the plane $y = 0$, ideally the electric field lines impinges the surface perpendicularly. If one inserts a ground plane at $y = 0$ this assures that all the field components are in fact perpendicular to the plane. The horizontal electrical field component vanish.

Figure 3.10: One IRA having a ground plane. [13]

The ground plane is a conductor surface inserted in a horizontal plane. It mirrors the electric field on one of its sides. This makes it possible to use only half of the IRA in operation. The half IRA (HIRA) is to prefer for some feed impedances offering a better impedance match. The characteristic impedance of the two-feed arm, transmission line is [38]

$$Z_c = Z_0 f_g \ [\Omega], \tag{3.11}$$

where the impedance of free space

$$Z_0 = \sqrt{\frac{\mu}{\epsilon}} \ [\Omega], \tag{3.12}$$

the geometrical impedance factor

$$f_g = \frac{K(m)}{4K(1-m)}, \tag{3.13}$$

$K(m)$ are the complete elliptical functions, and the parameter m is defined according to Equation 3.3. The HIRA is the preferred configuration of the antenna for certain values of the feed impedance. But for the IRA developed during this project, we have chosen not to include a ground plane.

The incorporation of a ground plane in the IRA provides mechanical sturdiness. At the feed point there are cable stubs; slim conductors on which the large feed arms are resting. This puts a lot of stress on the conductors which become sensitive to vibrations. Thus, the IRA becomes difficult to move and operate since every movement of the antenna add stress on the conductors. The ground plane reduces the stress and makes the antenna more sturdy.

Another benefit from including a ground plane are a change of the feed configuration. If the ground plane is included, then it is possible to let the coaxial cable run along the plane to make a smooth sweep as it meets the feed point. This would launch the electromagnetic wave in the direction towards the reflector and hence lower reflections shown in the TDR [13].

3.7.2 Splitter Balun

In ref. [14] the splitter balun is the device which provides a transformation of a signal propagating inside a 50 Ω, coaxial cable, to two signals propagating in two, different 100 Ω, coaxial cables. This enables slimmer feed arms and thus a lowered aperture blockage due to the smaller physical size of the arms. The type of splitter balun is specified by ratios, as for the one mentioned above, it is a 1:2 splitter balun. However, one other common value is 1:4, for the IRA application. Due to the complexity of the device it was not considered for the IRA developed during this project.

The inclusion of a splitter balun in the configuration of an IRA deteriorates the TDR. The device cause unwanted reflections in the circuit. Therefore, lots of effort has been put into improving the splitter in order to lower reflections. In both ref. [13] and [14] they provide data from experiments with improved splitter balun, all revealing flatter TDRs. As for the splitter in ref. [14] it is also adjusted to suit the high-voltage application by filling the void inside the splitter balun with a dielectric to prevent electrical breakdown.

Chapter 4

The Modelling

4.1 The Software - CST Microstripes 2009

The software used in the modelling of the antenna is CST Microstripes 2009. Microstripes was chosen as a simulation tool due to its superior properties when dealing with systems such as the IRA. The short impulse, and the preferred time domain analysis were the evaluated factors. CST Micrsostripes handles both considerations better than COMSOL Multiphysics which was the other evaluated software. COMSOL do not provide the required time domain analysis.

CST Microstripes is based on the transmission line matrix (TLM) method. It is a general, numerical method suitable for field problems. There is one fundamental difference between the TLM method and most numerical methods. When others uses an idealized continuous model which is solved exactly, the TLM method introduces the approximations in the first stage. The first stage is the discretisation stage, when portions of the material in the structure is substituted with transmission lines. The substitution proceeds until the whole structure comprises a network of transmission lines. Then the TLM is defined, and the system is solved.

At the initial discretization stage, portions of the media is substituted by transmission lines and nodes. The nodes are the transmission line intersections. The voltage and current at the nodes are used to calculate the electric and magnetic fields around the antenna in the model. The specific node used in CST Microstripes is the symmetrical condensed node (SCN) which has the advantage of introducing symmetry into the calculations and decreases the computational effort. The condensed character of the node imply that the field components are evaluated from the parameters, voltage and current, determined at the same point in all of the nodes, namely at the centre of the nodes [36].

The TLM method simplifies the complex electromagnetic problem significantly. The continuous process of electromagnetic wave propagation becomes propagation

and scattering of discrete electric and magnetic pulses inside a mesh of interconnected transmission lines. The software CST microstripes which implements the TLM method, can handle the short duration of the impulse, and the analysis is performed in time domain which makes it the optimal choice for the application of the IRA [43].

4.2 Developing the Model

The objective of the modelling is to capture the behaviour of the real-world antenna. Adjustments made in the model, in order to optimize the performance of the IRA, are to be applied to the constructed IRA such that optimal performance will be obtained. The optimization parameter is the magnitude of the electric field on boresight. The magnitude of the electric field is to be maximized.

The model requires a suitable solution for the different components and occurrences in the IRA. The main concerns of the IRA configuration are

- the reflector,
- the excitation,
- the coaxial cable,
- the junction between the feed arms and the reflector,
- the boundary conditions, and
- the material.

This section will describe the evolution of the IRA geometry when effective solutions for the above-listed concerns are found. The model evolved from a four-arm IRA fed by a coaxial port at origo (Figure 4.1(a)), to the canonical problem of an IRA fed by a wire port using efficient boundary conditions (Figure 4.1(d)) to decrease computer computational effort. This section will finish with a summary which lists the solutions for the considerations in a concise and efficient manner.

4.2.1 Reflector

The reflector of the IRA is created in two steps; first defining a parabola by using parametric relations governing the spatial coordinates, then second to rotate the parabola with respect to one axis in order to create a paraboloid surface. The

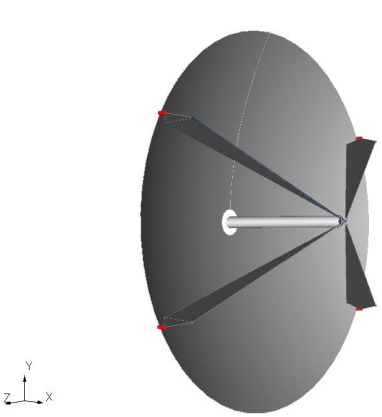

(a) The original model.

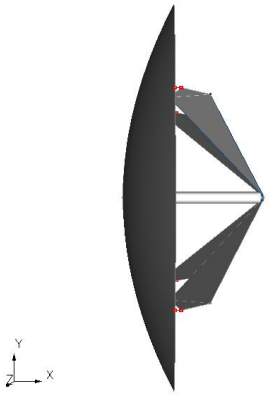

(b) The original model.

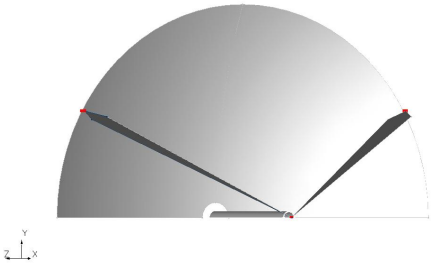

(c) The model using the electric wall.

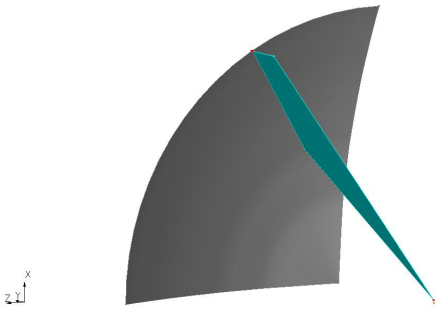

(d) The model using both the electric and the magnetic wall.

Figure 4.1: The evolution from a four-arm reflector fed by a coaxial port at origo, to the canonical model of the antenna fed by a wire port at the focal point using efficient boundary conditions.

relations governing the spatial coordinated are

$$x(u,\nu) = a\sqrt{\frac{u}{h}}\cos\nu, \tag{4.1}$$

$$y(u,\nu) = a\sqrt{\frac{u}{h}}\sin\nu, \tag{4.2}$$

$$z(u,\nu) = u, \tag{4.3}$$

where the angle $\nu = \pi/2$, the parameter $u \in [0.001, 0.20]$ m, the radius $a = 0.76$ m, and the height $h = 0.20$ m. The parabola is then rotated around the appropriate axis.

The ideal, paraboloid reflector was used in the initial simulations. However, the surface of the reflector used in the construction of the IRA contained surface errors.

There was a relatively large deviation of the reflector from the paraboloid. Therefore the reflector needed to be defined in another way. The reflector was measured. The reflector dept was probed along one axis connecting two opposite points one the reflector circumference. The coordinates were interpolated to obtain a paraboloid which resembled the reflector better than the ideal paraboloid defined by the spatial relations in Equations 4.2-4.3. As a remark, the coordinates measuring error due to the steel mesh of the reflector are relatively large. However, it is smaller than the overall reflector-deviation; motivating the use of interpolated coordinates. The coordinates are listed in Table 4.1.

Table 4.1: The coordinates measured along an axis connecting two opposite points on the circumference of the reflector. The coordinates interpolated to define the parabola which is axially rotated to create the reflector surface.

x	0	135	185	235	285	335	385	435	485
y	302.5	286	279.5	272.5	263	249	235	220	201
x (cont.)	535	585	635	685	735	785	835	885	
y (cont.)	181.5	163	138	113.5	86.5	59	31.5	0	

4.2.2 Excitation

The most complicated consideration of the antenna is that of the excitation. The excitation occur through ports defined in the model. Initially the port was positioned at origo; a coaxial port. The TEM wave propagate from the origo, through the coaxial cable, and onto the reflector directed by the feed arms. At the focal point, the coaxial cable meets the feed arms as seen in Figure 4.3(a). Unfortunately the simulation notes for this geometry revealed a high degree of reflections[1]. A smoother transition from the coaxial cable to the antenna were tried, seen in Figure 4.3(b). However, the attempt was not successful due to the remaining high degree of reflections and was thus abandoned.

In the next configuration the excitation was moved from the origo to the focal point and the coaxial port was replaced by a wire port. Different configurations were tested and the one most accurate which also was the one with the simplest configuration was chosen. Namely, that of the wire connected directly to the feed arm seen in Figure 4.3(f).

[1]These results will not be displayed due to their trivial appearance. The S_{11} parameter approximately attained the constant value 1 throughout the frequency interval of interest.

As for the magnitude of the excitation there are several options provided in the software. The ones used in this work are either the default impulse or the transient. The default is an arbitrary impulse determined by the software. The default impulse will be used to generate those modelling results for which the absolute magnitude is not the important parameter; when the relative magnitude of the modelling results are important. The use of the default impulse will merely emphasize the relative difference in magnitude between simulation results.

The transient pulse is that of a double exponential with a rise time of 1-2 ns, a time of decay of 3-4 ns, and a peak voltage of 90 kV. The transient is the preferred excitation signal for those results where their absolute magnitudes are compared. The signal resembles the signal which is produced by the FPG 90. The voltage waveform is seen in Figure 4.2.

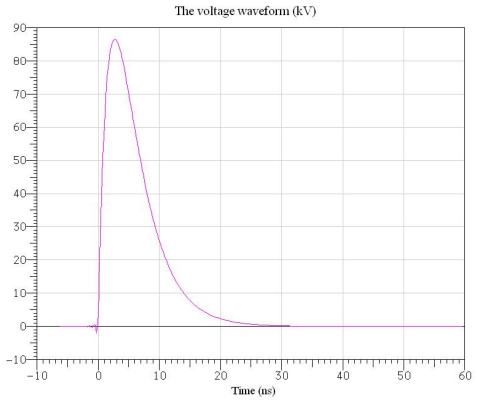

Figure 4.2: The voltage in the wire.

4.2.3 Coaxial Cable

Initially the IRA was excited through a coaxial port positioned at the origo. Then the signal propagated inside a coaxial cable and onto other parts of the antenna. When the excitation was moved from the origo to the focal point, the outer conductor of the coaxial cable was kept. During operation surface currents are induced on the surface of the outer conductor giving rise to a diffractive field. The constructed IRA will have a coaxial cable running from the rear of the antenna to the focal point. Induced surface currents will give rise to a diffractive field. In order to capture this behaviour in the model the outer conductor of the coaxial cable is detained during several simulations.

Unfortunately, the outer conductor of the coaxial cable in the model IRA made the model large. The computer managed only a relatively large mesh than what could have been possible without the outer conductor. This prohibited a conver-

gence analysis of the results. Therefore the outer conductor was removed to enable a finer mesh. The model assured more accurate results without it.

Another feature which motivates the removal of the outer conductor of the coaxial cable was the choice of material. The type of material do not give rise to the diffractive field caused by the interaction between the field and the components. The electromagnetic field will give rise to induced surface currents which are the origin of the diffractive field component. For the specific type of material there will not be any induced currents which give rise to the diffractive field. Therefore the outer conductor is once again an excessive part which can be removed.

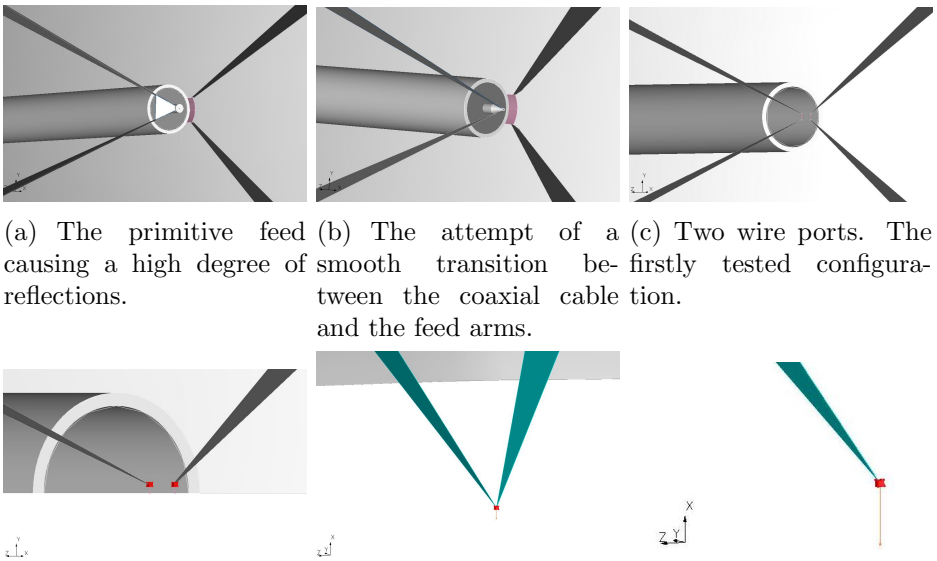

(a) The primitive feed causing a high degree of reflections.

(b) The attempt of a smooth transition between the coaxial cable and the feed arms.

(c) Two wire ports. The firstly tested configuration.

(d) Two wire ports. The secondly tested configuration.

(e) Two feed arms connected to the wire port.

(f) The feed of the model which generated the best results.

Figure 4.3: A close-up of the focal point.

4.2.4 Resistive Terminations

Another important feature of the model is the junction between the feed arms and the reflector. The junction comprise two cubes with one wire in between. The cubes are present due to problems arising in the discretization. If one is to use solely the wires as connections between arms and reflector, the discretization would cause the wires and the reflector/feed arms to detach. At first when this problem arose, a local, finer mesh was tested. However, this caused errors when the diameter of the wire became too large in comparison to the cell size. Therefore, the cubes were

introduced. They function well in filling the void in the junction caused in the discretization. A close-up of the arrangement can be seen in Figure 4.4.

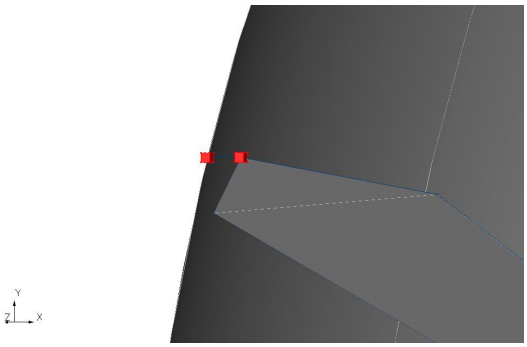

Figure 4.4: A close-up of the junction between the feed arms and the reflector. The junction consists of two cubes connected with one wire.

4.2.5 Boundary Conditions

The four-arm IRA shown in the uppermost images in Figure 4.1 defines a large model. Due to the short duraion of the pulse the model requires a fine mesh in order to generate satisfying results. This calls for a lot of computational power. With such a model it is not possible to conduct a convergence analysis. Thus, one cannot tell anything about the accuracy of the results. Therefore a lot of effort has been made to decrease the required computational effort of the model, in order to enable a convergence analysis.

To reduce computational effort the use of boundary conditions are essential. In the most efficient model of the IRA there are two boundary conditions in use as seen in Figure 4.5; the electrical wall boundary and the magnetic wall boundary. The former is a boundary condition which is in favour at boundaries where the electrical field components are all normal to the boundary in question. The magnetic wall is to the magnetic field what the electric wall is to the electric field; it is a boundary on which all magnetic field components are normal.

One understands the physical motivation of the boundary conditions when one looks at the electric field generated by two feed arms of different potential. The electric field at a horizontal plane equidistant from the two arms, is perpendicular to the plane. Therefore, the electric wall is inserted at the plane to which the electric field components are perpendicular.

4.2.6 Material

There are two materials assigned to the IRA; the predefined lossless metal and the dielectric making the impedance of the coaxial cable equal to 75 Ω. As for the models which do not incorporate the coaxial cable, they comprise the lossless metal.

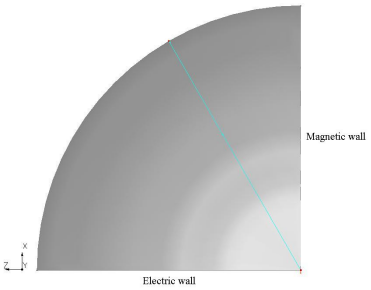

Figure 4.5: The boundary conditions in the most efficient IRA model.

The predefined lossless metal found in CST Microstripes is an ideal material allowing for infinite conductance and a zero penetration depth. The former makes the material an infinitely good conductor. Having a zero penetration depth implies that the radiation from the IRA itself will not induce surface currents in the components. Therefore the produced electric field will not include any diffractive field component generated by surface currents.

The dielectric fills the void between the two conductors in the coaxial cable, in those models in which the cable is kept, is chosen in such a way that the characteristic impedance of the cable is equal to 75 Ω. This imposes a condition on the dielectric and the dimensions which need to satisfy the relation

$$Z_0 = \frac{1}{2\pi}\sqrt{\frac{\mu}{\epsilon}}\ln\frac{D}{d} = 75\Omega. \tag{4.4}$$

Where the parameters D [m] and d [m] are the outer and the inner diameter of the conductors, respectively. The dielectric material was then chosen to satisfy the above condition.

4.2.7 Summary

The model IRA which has been developed during this master thesis work uses efficient solutions for each of the above-listed considerations.

- The reflector is generated with interpolated coordinates gathered during measurements.
- The excitation occur through a wire port positioned at the focal point. The wire is connected directly to the feed arm, seen in Figure 4.3(f).
- The junction between the feed arms and the reflector is implemented in the model as a wire with the appropriate resistance, seen in Figure 4.4.

- The boundary conditions are the electric and the magnetic walls, seen in Figure 4.5.

- The material is a predefined lossless metal.

4.3 Results

The simulation results displayed in this section are either confirming expected results or determining an important characteristic of the IRA. The former type which confirm the expected behaviour of the IRA has been generated in order to assure that the model is functioning well. The results with this character are

- the radiation characteristics,

- the feed arm location,

- the included angle of the feed arms,

- the electric field independence of the focal point displacement[2], and

- the spectral magnitude of the electric field.

The simulation results which determine important parameter of the IRA are

- the terminating resistance.

The results will be used such that the IRA is designed in a way that assures the most optimal peak electric field strength on boresight.

4.3.1 Radiation Characteristics

The magnitude of the electric field was determined by simulations at ten different positions within the interval of 1 - 5 m from the focal point. The value of r and the magnitude of the electric field was used to determine the proportionality constant E_c in equation 4.6. For each constant the magnitude of the electric field was plotted. Ten curves is displayed in Figure 4.6. The model is excited with the default pulse incorporated in the software.

[2]It is independent in the sense that it does not vary within the interval of interest.

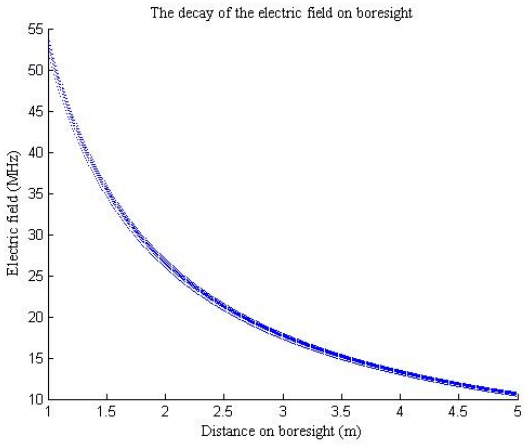

Figure 4.6: The simulated value of the electric field at points evenly distributed within the interval 1 - 5 m which display the $1/r$ decay as one moves in the direction away from the antenna.

4.3.2 Resistive Terminations

At the junction between the feed arms and the reflector there are wires in the model representing the resistors. The wires has assigned resistances to enable the resistive load. The resistance has been varied for several values relative the characteristic impedance of the transmission lines manifested in both the model and the constructed IRA by the feed arms. In Figure 4.7 the electric field strength at boresight is displayed for several values of the wire resistance; 27 %, 40 %, 50 %, 58 %, and 67 % of the characteristic impedance of the transmission line. The model is excited with the transient voltage pulse.

4.3.3 Feed Arms

The feed arms make an angle with the vertical symmetry line. Traditionally, due to symmetry, this angle has been 45°, but variations of this angle has showed an improved performance. The electric field strength is displayed in Table 4.2 for the three angles 30°, 45°, and 60° with the vertical symmetry line. The IRA is with the default pulse incorporated in the software.

Table 4.2: The peak electric field strength varying with the feed arm angle made with the vertical symmetry line.

Angle	Peak electric field strength (MV/m)
30°	5.161
45°	3.467
60°	2.147

4.3.4 Focal Point Displacement

The directivity as a function of focal point displacement was investigated at the particular frequency of 100 MHz. The directivity is displayed in dBi, it relates the radiation of the IRA with the radiation of an isotropic radiator. The values of the directivity at certain focal lengths are displyed in Table 4.3.

Table 4.3: The directivity with respect to a displaced focal point.

Focal length	Directivity
666	4.040
667	4.045
668	4.044
669	4.045
670	4.044
671	4.042
672	4.042
673	3.977
674	3.988
675	3.987
676	3.990

4.3.5 Spectral Magnitude of the Electric Field

The spectral magnitude of the electric field is seen in the Figures 4.3.5. The Figures probe the spectral magnitude of the electric field as a function of the frequency within the two intervals, 0-500 MHz, and 0.5-1 GHz. The IRA is excited with the default pulse incorporated in the software.

4.4 Discussion

The electric field in the far field region of the IRA is known to behave as [5, 9, 23, 41, 42, 15, 24]

$$\vec{E}(r,t) = \frac{D}{4\pi c f_g}\frac{1}{r}\left\{\frac{\partial V}{\partial t}(t-T) - \frac{1}{T}\left[V(t) - V(t-T)\right]\right\}. \tag{4.5}$$

Thus, we expect the magnitude of the electric field on boresight to decay as $1/r$.

$$\vec{E}\,(r,t) = \frac{1}{r}E_c \tag{4.6}$$

Ten different values of the constant E_c has been determined by simulations. Ten curved has been plotted in Figure 4.3.5. The curves approximately coincide which confirm the expected decay of the electric field strength.

The theoretically determined spectral magnitude of the electric field of the IRA is seen in Figure 2.10(a). It should be noted that the spectral magnitude of the electric field in the graph is the Fourier transform of the electric field in time domain, the spectral magnitude having the unit [Vs/m]. The electric field in the frequency domain, in the unit [mV/m], from the simulation is seen in Figure 4.3.5.

The theoretically determined spectral magnitude of the electric field in the region of 0-1 GHz is a smooth curve. But the simulated magnitude of the electric field show periodic dips with a period of 225 MHz. Due to the periodicity of the occuring dips one believes that the origin is the illumination of the reflector. The feed arms illuminate the reflector in such a way that certain periodic frequencies is not transmitted with the same intensity as the rest. Therefore there are dips with the periodicity.

The excitation of the model from which the results are collected is not made with the transient in Figure 4.2. It is made with the default signal produced by the software. Therefore one cannot tell anything about the quantitative magnitude of the electric field. As for the qualitative behaviour, if one take into the account of the periodic dips, one sees that the simulated magnitude of the electric field increases in the frequency interval which resembles the theoretically determined spectral field.

When we measured the reflector used in the construction of the IRA, we found that its surface deviated greatly from that of a paraboloid defined with the same diameter D and F/D ratio. Therefore, the surface of the paraboloid used in the modelled IRA is interpolated from coordinates determined by measurements made on the reflector. This required an investigation of the most optimal focal point. The directivity of the IRA is influenced by focal point displacement. Therefore the directivity with respect to a focal point displacement was determined by simulations. A model for each millimetre within the range of 666 - 676 mm was defined. The reason for using this interval was simply that it included the original focal point of the reflector based on information offered by the manufacturer.

In Figure 3.6 we saw that one required a relatively large focal point displacement in order to affect the radiated electric field for the frequency range in which we are interested. The simulation confirmed it. The directivity within the range of 666-676 mm is rather constant. The results is seen in Table 4.3. The lowest value of the directivity is 98 % of the highest value which makes them approximately equal.

The feed arms make a 30° angle to the vertical. This has proven successful in many experiments. To confirm this value three different models has been determined, differing in the feed arm angle to the vertical; 30°, 45° and 60°. The peak of the magnitude of the electric field is listed for the three designs. The electric field strength is 5.161 MV/m, 3.467 MV/m, and 2.147 MV/m, respectively. The models has been excited with the default pulse incorporated in the software. Therefore, the actual numerical values do not tell anything. However, their relative dependence do. The highest magnitude of the electric field was obtained with the 30° angle to the vertical.

The radiated electric field of the manufactured IRA will have the characteristic appearance of Figure 2.11. However, the radiation of the modelled IRA will be slightly different due to a difference in excitation. The excitation of the manufactured IRA will give rise to a negative prepulse of the length

$$\frac{2F}{c} \ [s] \tag{4.7}$$

which is created when the TEM wave is launched; one part propagates toward the reflector and the other part propagates in the direction of boresight. The prepulse is then launched toward the observer. The length of the prepulse is determined by the duration of a TEM wave propagating two focal lengths; one in direction toward the reflector and one away. Thus the impulse will reach the observer with a time delay. The excitation of the modelled IRA occurs through a wire port. It gives rise to the TEM wave travelling towards the reflector due to the potential difference applied to the feed arms. Therefore, the prepulse of the radiation of the modelled IRA is absent.

The impulse of the electric field component displayed in the Figures 4.7 are within the range 48-53 V/m. The interesting feature of the radiation are that of the tail. For a certain transmission line impedance T, it is favourable to choose the terminating resistance equal to $T/2$ in order to minimise the reflections in the circuit. Unfortunately, this situation align the electric and magnetic dipole moments of the antenna in an undesired direction. Therefore one should choose another terminating impedance.

In Figure 4.7(c) we have the terminating impedances equal to half that of the transmission line. The peak of the impulse is 53 V/m, the initial dip of the tail is -33 V/m. The overall radiation is satisfactory. In Figure 4.7(d) and 4.7(e), one sees that the width of the dip occurring just after the impulse is smaller than the one seen in Figure 4.7(c). Small widths are preferable since it allows for higher peaks. Therefore, one can conclude that the terminating resistance should attain a value which is around 58 % of the impedance value of the transmission line. The peak of the impulse in Figure 4.7(c) is larger than that of Figure 4.7(e), therefore 67 % might be the most preferable terminating impedance.

It is difficult to deduce the actual peak value of the electric field since it depends on the mesh. Due to a lack of computer memory, the used mesh was rather coarse. A convergence analysis, were one refine the mesh in each step until one get a stable value of the electric field strength, enabled peak electric field strengths which started stabilizing. To be certain, one needs an even finer mesh to confirm the convergence analysis. But this was not possible due to the lack of computer memory. Therefore the actual values of the peak electric field cannot be determined by simulations.

Another feature to consider of the electric field component is that the positive contributions of the electric field component should belong to the impulse. A clearly, unwanted situation is seen in Figures 4.7(a) and 4.7(b). The impulse is followed by two dips, the later shallower than the first. Thereafter one can see another peak, a contribution in the positive component direction, not belonging to the impulse. Due to the first constraint of the IRA radiation (Equation 2.19), this lowers the impulse. Hence the terminating resistance should not be less than half the impedance of the transmission line.

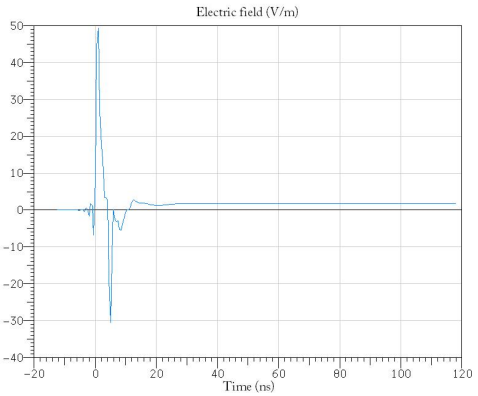

(a) 27 %.

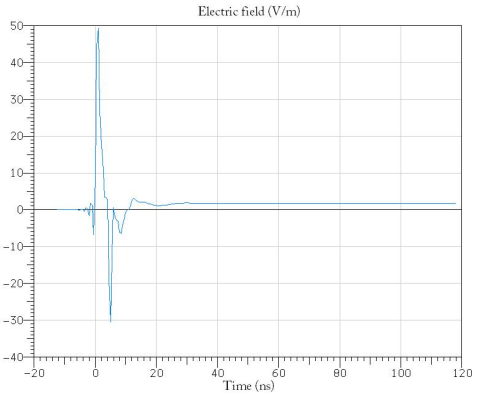

(b) 40 %.

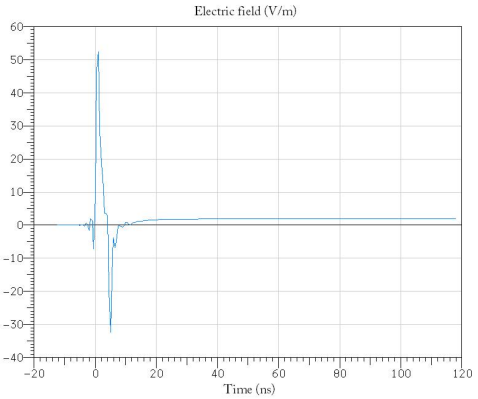

(c) 50 %.

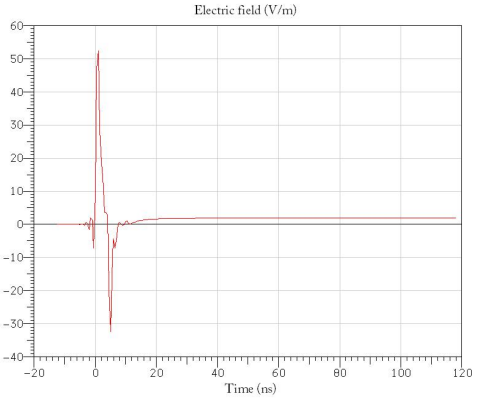

(d) 58 %.

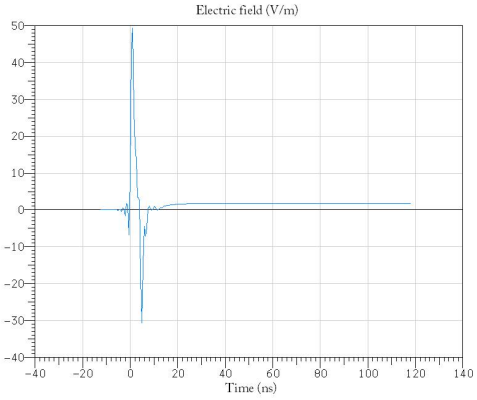

(e) 67 %.

Figure 4.7: The electric field strength when the terminating resistance is 27 %, 40 %, 50 %, 58 %, and 67 % of the transmission line impedance.

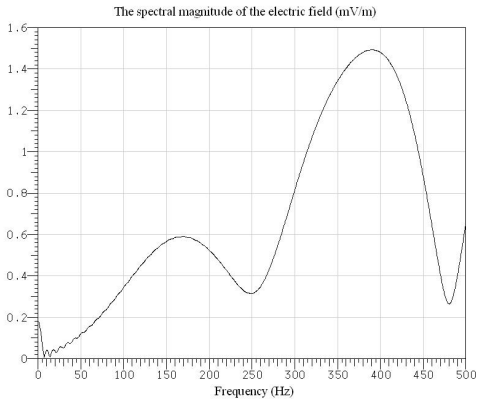

(a) The frequency interval 0-500 MHz.

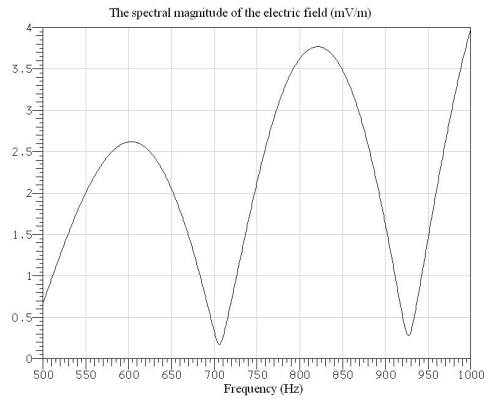

(b) The frequency interval 0.5-1 GHZ.

Figure 4.8: The spectral magnitude of the electric field [V/m].

Chapter 5

Discussion and Conclusion

5.1 Discussion

The objective of this master's thesis work was to suggest a suitable geometry of the impulse-radiating antenna for the high voltage operation of 90 kV, by research and modelling.

The IRA design takes several phenomena into consideration;

- electrical breakdown due to the high voltage excitation,
- impedance matching such that the power transmission will proceed effectively,
- the electric and magnetic dipole in order to optimize the radiation, and
- diffractive effects which alter the appearance of the transmitted impulse.

In order to prohibit electrical breakdown during antenna operation, the distance between conductors is kept large. The interface between the dielectric of the coaxial cable and air has a threaded shaped to provide a long surface path such that a conductive path between the cathode and anode is not formed. Such a path would cause surface electrical breakdown. Another included, structural feature are the rounded edges, since sharp peaks tend to accumulate charges and should therefore be avoided. As a suggestion for future work; critical areas having an imminent risk of electrical breakdown can be modelled. A static voltage excitation applied to the conductors would reveal the actual electric field strengths involved. The model would also tell where the electric field strength is larger. With this knowledge one can focus on improving the design of these particular areas. In the IRA developed during this project, the risk of electrical breakdown has been removed by using threaded-shaped interfaces, also the IRA could be operating inside a container filled with some gas having a larger dielectric strength than that of air.

The topic of impedance matching is important. An matched circuit will effectively transmit power, and power loss due to reflections in the circuit is kept minimal. The feed arm pairs which are the transmission lines from the splitter to the air has been adjusted. Their included angle determine their characteristic impedance which is matched to the output impedance of the splitter.

The electric and magnetic dipole moments are aligned by varying the terminating resistance at the junction between the feed arms and the reflector. The modelling revealed that the terminating resistance should be slightly larger than half the value of the characteristic impedance of the feed arm pairs. In a future project, it could be possible to treat the instantaneous heating of the resistors. There are several softwares provided for the analysis of a circuit, for instance SPICE. Such a circuit analysis could deduce the actual currents inside the resistors causing the heating. The results then motivate a suitable resistor type. In this project we have used resistors recommended by experienced and qualified users. But the choice can made more sophisticated.

Diffractive effects such as feed arm edge interaction, and reflection rim interaction alter the appearance of the transmitted pulse as it passes the antenna. These effects are difficult to remove completely. But it is possible to limit the effect by the use of slim feed arms which cause little aperture blockage. Slim feed arms will cause an impedande mismatch with the transmission lines. Thus one will need to balance between the two conditions. For the IRA developed during this project the impedance matching govern the geometry of the feed arms.

The simulation notes need to be confirmed by experimental testing. Unfortunately, the tests of the IRA has been postponed until the fall of 2009 and will not be included in this master thesis. As a guidance of the antenna capability, one IRA developed by D. V. Giri [23] generates an electric field strength in the order of 4.2 kV/m at a distance of 304 m.

5.2 Future Work

There are mainly two areas in which future work can be done;

- The choice of resistors, and
- the modelling of the surface electrical breakdown.

The choice of resistors is critical. The high voltage excitation cause a relatively high current to pass through the resistors at the junction between the feed arms and the reflector. The current induce an instantaneous heating of the device. The heating can lead to a burnout of important traces inside the resistors, and cause breakdown of the overall device. It is possible to model the antenna as a circuit in a software

such as SPICE. The modelling reveals the peak current inside the resistors. Then one uses this as basis in the choice of resistors.

The combined interface between the coaxial cable and air is a critical area suffering from the risk of surface electrical breakdown. There is a risk that a conducting path along the surface is formed between the cathode and the anode during operation. In order to estimate the voltage giving rise to such a breakdown it is possible to use CST Microwave Studio in the development of a suitable design. A static voltage excitation applied to the conductors estimates the involved electric field strengths. The model also determines where the electric field intensity is higher. With this knowledge one can focus on improving the design of these particular areas.

5.3 Conclusion

The IRA developed during this master thesis work is suitable for the application of IEMI. It is a high voltage application, and the additional strain on the structure imposed by the high voltage pulse will be dealt with using designed interface. The positioning of the electric, and magnetic dipoles, *id est* the terminating resistance, was determined by simulations. And, the included feed arm angle is adjusted in order to obtain impedance matching in the overall circuit.

Bibliography

[1] Denny Aberg. System engineer at BAE Systems Bofors. *Discussions during the time period of this thesis*, 2009.

[2] Constantine A. Balanis. *Antenna theory - Analysis and design.* John Wiley and sons, 2005.

[3] C. E. Baum, W. L. Baker, W. D. Pratcher, W. A. Walton III, R. Hackett, J. M. Lehr, J. W. Burger, R. J. Torres, J. O'Loughlin, H. A. Dogliani, J. S. Tyo, J. Schoenberg, G. J. at Air Force Research Laboratory Rohwein, D. V. at Pro-Tech Giri, I. D. Smith, R. Altes, G. Harris, J. Fockler, D. F. at Titan Pulse Sciences Morton, D. McLemorem, K. S. H. Lee, T. Smith, H. at ITT Industries LaValley, M. D. Abdalla, F. Skipper, M. C. at ASR Corporation Gruner, B. at Kinetech Cockreham, and E. G. at Farr Research Inc. Farr. Review article. *Sensor and Simulation Note 480*, 2003.

[4] Carl E. Baum. Optimizing the feed impedance of impulse radiating antennas part I: Reflector IRAs. *Sensor and Simulation Note 354*, 1993.

[5] Carl E. Baum. Selection of angles between planes of TEM feed arms of an IRA. *Sensor and Simulation Note 425*, 1998.

[6] Carl E. Baum. Symmetry in single-polarization reflector impulse radiating antennas. *Sensor and Simulation Note 448*, 2000.

[7] Carl E. Baum. Some topics concerning cable feeds of reflector IRAs. *Sensor and Simulation Note 462*, 2001.

[8] Carl E. Baum. Email correspondence during the time period of the master's thesis, 2009.

[9] Carl E. Baum, Everett G. Farr, and Charles A. Frost. Transient gain of antennas related to the traditional continuous-wave (CW) definition of gain. *Sensor and Simulation Note 412*, 1997.

[10] James Becker, Dejan Filipovic, Hans Schantz, and Seong-Youp Suh. Ultrawideband antennas. *International Journal of Antennas and Propagation*, 2008.

[11] James Benford, John A. Swegle, and Edl Schamiloglu. *High power microwaves*. Taylor and francis group, 2000.

[12] Leland H. Bowen and Everett G. Farr. Experimental results of optimizing the location of feed arms in a collapsible IRA and a solid IRA. *Sensor and Simulation Note 450*, 2000.

[13] Leland H. Bowen and Everett G. Farr. Results of optimization experiments on a solid reflector IRA. *Sensor and Simulation Note 463*, 2002.

[14] Leland H. Bowen and Everett G. Farr. A high-voltage cable-fed impulse radiating antenna. *Sensor and Simulation Note 507*, 2005.

[15] Leland H. Bowen, Everett G. Farr, and William D. Prather. Fabrication and testing of two collapsible impulse radiating antennas. *Sensor and Simulation Note 440*, 1999.

[16] David K. Cheng. *Field and Wave Electromagnetics*. Addison and Wesley, 1992.

[17] Electronic communications committee. ECC decision of 24 march 2006 amended 6 july 2007 at Constanta on the harmonised conditions for devices using UWB technology in bands below 10.6 GHz. *(ECC/DEC/(06)04)*, 2007.

[18] Everett G. Farr. Email correspondence during the time period of the master's thesis, 2009.

[19] Everett G. Farr and Carl E. Baum. Radiation from self-reciprocal apertures. *Sensor and Simulation Note 357*, 1993.

[20] Everett G. Farr and Carl E. Baum. Time domain characterization of antennas with TEM feeds. *Sensor and Simulation Note 426*, 1998.

[21] Everett G. Farr, Carl E. Baum, and William D. Pratcher. Multifunction impulse radiating antennas: Theory and experiments. *Sensor and Simulation Note 413*, 1997.

[22] Gerald B. Folland. *Fourier analysis and its applications*. Brooks/Cole publishing Company, 1992.

[23] D. V. Giri. Radiated spectra of impulse radiating antennas (IRAs). *Sensor and Simulation Note 386*, 1995.

[24] D. V. Giri and Carl E. Baum. Reflector IRA design and boresight temporal waveforms. *Sensor and Simulation Note 365*, 1994.

[25] D. V. Giri and S. Y. Chu. On the low-frequency electric dipole moment of impulse radiating antennas. *Sensor and Simulation Note 346*, 1992.

[26] D. V. Giri, T. K. Liu, F. M. Tesche, and R. W. P. King. Parallel plate transmission line type of EMP simulators: A systematic review and recommendations. *Sensor and Simulation Note 261*, 1980.

[27] D. V. Giri and F. M. Tesche. Classification of intentional electromagnetic environments (IEME). *IEEE EMC Transactions special issue paper*, 2003.

[28] P. G. Ingerson and W. V. T. Rusch. Radiation from a paraboloid with an axially defocused feed. *IEEE Transactions on antennas and propagation*, 1973.

[29] Oleg D. Jafimenko. *Electricity and magnetism: An introduction to the theory of electric and magnetic fields*. Electric Scientific, 1989.

[30] Mats Jansson. System engineer at BAE Systems Bofors. *Discussions during the time period of this thesis*, 2009.

[31] Magnus Karlsson. System engineer at BAE Systems Bofors. *Discussions during the time period of this thesis*, 2009.

[32] F. H. Kreuger. *Industrial high voltage*. Delft University Press, 1991.

[33] Monsef Larbi. Design of an ultra-wideband antenna for high power applications - time-domain simulations and construction of an optimized TEM horn antenna. *Examensarbete*, 2006.

[34] Wikipedia on the topic of Penetration depth. Available at: `http://en.wikipedia.org/wiki/Penetration_depth`, 2009-04-28.

[35] Ian Oppermann, Matti Hmlinen, and Jari Iinatti. *UWB: Theory and Application*. John Wiley and Sons, incorporated, 2005.

[36] J. A. Port and J. A. Morente. A three-dimensional symmetrical condensed TLM node for acoustics. *Journal of Sound and Vibration*, 2001.

[37] Lennart Rade and Bertil Westergren. *Mathematics handbook for science and engineering*. Studentlitteratur, 2004.

[38] F. Sabath, D. Nitsch, M. Jung, and Th. H. G. G. Weise. Design and setup of a short pulse simulator for susceptibility investigations. *Sensor and Simulation Note 460*, 2001.

[39] Hans Schantz. *The art and science of UWB antennas.* Artech house, 2005.

[40] Agilent Technologies. Improving TDR/TDT measurements using normalization. *Application Note 1304-5*, 2001.

[41] J. Scott Tyo. Optimization of the TEM feed structure for four-arm reflector impulse radiating antennas. *IEEE Transactions on antennas and propagation, no. 4*, 2001.

[42] J. Scott Tyo, Everett G. Farr, Leland H. Bowen, and Larry L. Altgilbers. IRA variations useful for flexible feed arms. *Sensor and Simulation Note 472*, 1994.

[43] The webpage of the software CST Microstripes. Available at: `http://www.cst.com/Content/Products/MST/Overview.aspx`, 2009-04-28.